IEEE Access
Multidisciplinary ⋮ Rapid Review ⋮ Open Access Journal

Received November 21, 2020, accepted November 26, 2020, date of publication November 30, 2020,
date of current version December 14, 2020.

Digital Object Identifier 10.1109/ACCESS.2020.3041398

Dynamic Reconfiguration of Multiobjective Distribution Networks Considering DG and EVs Based on a Novel LDBAS Algorithm

JIE WANG[1], WEIQING WANG[1], HAIYUN WANG[1], AND HUIWEN ZUO[2]

[1]Engineering Research Center of Education Ministry for Renewable Energy Power Generation and Grid-Connected Control, Xinjiang University, Urumqi 830047, China

[2]Shanghai Research Institute of Aerospace Computer Technology, Shanghai 201109, China

Corresponding author: Weiqing Wang (wangwq666@gmail.com)

This work was supported in part by the National Natural Science Foundation of China under Grant 52067020, in part by the Autonomous Region Government under Grant 2018D04005, in part by the Key Natural Science Projects of Universities under Grant XJUBSCX-201904, and in part by the Natural Science Foundation of Xinjiang Autonomous Region under Grant 2020D01C068.

ABSTRACT Aiming to improve the operation economy and power quality of distribution systems subject to the fluctuating and stochastic power outputs of distributed generation (DG) units and electric vehicles (EVs), a multiobjective optimization model for network reconfiguration and its corresponding solution method are proposed. First, a dynamic reconfiguration model is constructed based on the power loss rate (PLR) as well as the active power loss, the load balancing index and the maximum node voltage deviation, which serve as the optimization indexes. Second, the Lévy flight and chaos disturbed beetle antennae search (LDBAS) algorithm is presented based on the grey target decision-making technique, which can not only improve the computational efficiency but also find the most satisfactory solution for the proposed dynamic reconfiguration model. Considering the uncertainties of loads and DG outputs, the influence on the load curve of EV connecting to the distribution network at different penetration rates and under different charging/discharging modes is analysed. Additionally, the modified IEEE 33-bus and 118-bus test radial distribution networks are simulated to verify the effectiveness and superiority of the presented reconfiguration model and the improved LDBAS method, and the results illustrate that the proposed reconfiguration method can improve the operation economy and power quality of the distribution system and encourage the penetration of EVs.

INDEX TERMS Distribution system, time-varying characteristics of DGs and EVs, dynamic reconfiguration, multiobjective optimization, grey target decision-making, LDBAS algorithm.

I. INTRODUCTION

With the advent of the green grid concept, the high-level penetration of distributed generation (DG) and electric vehicle (EV) charging loads is introducing new problems affecting the dispatching operations of distribution networks. On the one hand, the outputs of DG units depend on climate factors such as wind and solar radiation and exhibit fluctuations and intermittency [1], placing high requirements on the adaptability and control of distribution networks. On the other hand, batteries for EVs can be used as energy storage devices to reduce the power fluctuations caused by DG and provide reliable auxiliary system services, thus improving the flexibility of distribution network operation [2].

The associate editor coordinating the review of this manuscript and approving it for publication was Salvatore Favuzza.

Distribution systems generally have the characteristics of a closed-loop structure and open-loop operation [3]. Optimal reconfiguration (OR) for distribution system operation, that is, changing the topological structure of the network by changing the open/closed states of the switches under operating conditions, can reduce the power loss, balance the load and improve the voltage quality to improve the operation performance, thus playing an important role in the optimal operation of distribution systems [4]. Power loads themselves show a certain level of randomness, and DG units and EVs connected to the distribution network introduce more power fluctuations and uncertainty. Accordingly, it is necessary to research projects in which the method of distribution system reconfiguration considers DG units and EVs simultaneously to improve the power quality and economic performance of power distribution systems during operation

and promote the acceptance and utilization of renewable energy.

The dynamic reconfiguration of a distribution network involves optimization in both time and space, and the solution process needs to consider various actual constraints, such as switch operation constraints, in addition to the various uncertain parameters discussed above when solving the reconfiguration model [5]–[8]. In [9], a comprehensive evaluation index was proposed based on the network loss and voltage offset after dynamic reconfiguration. This work also considered the period during which the standard deviation of the comprehensive evaluation index is less than a certain threshold value. In [10], [11], the dynamic reconfiguration method based on dynamic clustering with root data negative load waves was proposed. In [12], an intra-day dynamic reconfiguration method was explored based on the number of remotely controlled switches and their action times to minimize the operation cost of the distribution network. In [13], a dynamic reconfiguration method was constructed based on a minimum return threshold, combined with two adjacent periods when the difference in the evaluation function is less than the minimum return value. In [14], a state-based sequential network reconfiguration strategy was proposed by using a Markov decision process model, and an approximate dynamic programming approach was used to overcome the curse of dimensionality caused by the enormous numbers of states and actions. However, the above study have the following three deficiencies: (1) The method used to divide the reconfiguration periods in accordance with load fluctuations cannot guarantee the OR scheme throughout the whole reconfiguration cycle. (2) The segmentation method based on time periods suffers from subjectivity. (3) The reconfiguration model of the distribution system considers only the fluctuations in the DG outputs and does not consider EVs. In particular, it is necessary to achieve dynamic reconfiguration based on the power loss rate (PLR), which is a comprehensive index used to evaluate the economic operation and technical management of a power grid.

Furthermore, dynamic reconfiguration is a high-dimensional nonlinear combinatorial optimization problem involving a complex space-time distribution. Accordingly, the studied solution methods include mathematical optimization methods [15], [16], optimal flow mode methods, switch exchange algorithms and artificial intelligence algorithms from the perspective of optimization as well as both single-objective optimization methods and multiobjective optimization methods. In [17], a reconfiguration model for a distribution system was established based on optimal power flow, and a solution method was proposed based on a decoupling technique. In [4], a heuristic distribution system reconfiguration method was proposed to minimize the network loss. Among intelligent algorithms, the firefly algorithm has been used to solve the optimization problem for distribution network reconfiguration considering the objective of power loss minimization [18], [19]. In [20]–[23], the tabu search algorithm, an evolutionary programming algorithm, an improved cuckoo search algorithm, and an improved genetic algorithm were proposed to overcome the problems of slow evolution and difficulty of stably converging based on various objectives, such as a minimum loss, minimum load equalization and switching mitigation for distribution network operation. In 2014, a non-dominated sorting particle swarm optimization (PSO) algorithm was proposed to find the best solution for distribution network reconfiguration, considering solar and wind generation as well as three objective functions of a maximum power loss, a maximum voltage deviation and a maximum number of switching operations [24]. Furthermore, a multiperiod distribution network reconfiguration model has been established considering a comprehensive objective function involving the network loss, operating cost and power loss, which was solved by using a hybrid algorithm combining PSO and the grey wolf optimizer [25]. In [26]–[28], to solve the optimization problem for the normal operation of a distribution network for all objective functions simultaneously, a non-dominated sorting genetic algorithm was improved based on fuzzy theory and a mathematical simplification process. In [29]–[31], a hybrid evolutionary algorithm for obtaining the best combination of on/off statuses of the switches was introduced for a distribution network considering DG from various aspects, such as time-varying electricity prices and different load levels as well as demand response services with objective functions of operation cost and power loss. Based on the above analysis, we find the following two deficiencies: (1) Artificial intelligence algorithms still face the problems of falling into local optima and poor convergence. (2) Multiobjective problems for distribution network reconfiguration suffer from subjectivity.

Therefore, in this study, a multiobjective dynamic reconfiguration model is proposed based on the PLR considering the variations in DG outputs and EV charging/discharging, offering a more suitable strategy for managing the practical operation of a modern distribution network system. The reconfiguration model allows the network to be reconfigured under two kinds of operating modes: OR (OR means that the topology changes only one time during reconfiguration hours) can be performed in the normal operating mode, or real-time reconfiguration (RTR, that is, topology will changes every hour during reconfiguration hours) can be performed to achieve fast response of the network topology under obvious fluctuations in the equivalent loads or DG outputs. In addition, to more efficiently find a satisfactory solution for the reconfiguration of the distribution network, the Lévy flight and chaos disturbed beetle antennae search (LDBAS) algorithm is proposed based on the use of the grey target decision-making technique to solve the problem of multiple conflicting objectives. In simple terms, the major contributions of this study are as follows:

1) A dynamic reconfiguration model considering DG and EVs is proposed that can ensure the security and reliability of a power distribution system.

2) To improve the computational efficiency and find the globally optimal solution, the Lévy flight and chaos disturbed mechanism are introduced into the optimization process of the original BAS algorithm for solving the proposed reconfiguration model with multiple objective functions.
3) A grey target decision-making method is used to rank the beetles corresponding to multiple conflicting objectives in order to better meet the actual needs of personnel.
4) Considering the uncertainties of the loads and DG outputs, the influence on the load curve of EVs connecting to the distribution network at different penetration rates and under different charging/discharging modes is analysed.

This study is described in the following sections. Section II discusses the patterns of the loads and DG outputs. Section III describes the mathematical problem of distribution network reconfiguration. Section IV introduces the modified LDBAS method and its application to the proposed reconfiguration model. Section V describes the numerical simulation for the proposed algorithm. Section VI reports simulation results based on the modified IEEE 33- and 118-bus test systems. Finally, section 6 presents the conclusions of this study.

II. LOAD AND DG PATTERNS

For the reconfiguration of a distribution network, the parameters with uncertain characteristics mainly include the charging/discharging loads of the EV groups, the DG outputs and the load capacity. It is also necessary to analyse the time variation of the comprehensive load, which will affect the power quality and operation economy of the distribution network.

A. WIND TURBINE OUTPUT

The average wind speed v of a wind farm in a certain period can be described by the Weibull distribution. When v is between the cut-in wind speed v_{ci} and the rated wind speed v_r, the active power P_w of the wind turbine output has an approximately linear relationship with V, as shown in the following formula:

$$P_w(v) = \begin{cases} 0 & v < v_{ci} \\ P_{rate}\dfrac{v - v_{ci}}{v_r - v_{ci}} & v_{ci} \le v < v_r \\ P_{rate} & v_r \le v < v_{co} \end{cases} \quad (1)$$

where P_{rate} represents the rated power of the wind turbines, v_{ci} represents the cut-in speed, and v_{co} represents the cut-out speed.

B. PHOTOVOLTAIC OUTPUT

A photovoltaic power generation system consists of photovoltaic panel units. Its output can be expressed as

$$P_{solar} = r\sum_{m=1}^{M} A_m\eta_m = rA\eta \quad (2)$$

where r represents the solar radiation, M represents the number of photovoltaic panel units, and A_m and η_m are the area of the mth photovoltaic panel unit and photoelectrical transformation efficiency, respectively.

C. LOAD PATTERN

Power users are generally classified as residential, industrial and commercial users. Then, the daily load curve P_{Li} for node 'i' can be expressed as

$$P_{Li} = \sum_{s\in S} P_{Ni}\theta_{si}\delta_s \quad (3)$$

where $S = \{s|1, 2, 3\}$ represents the set of power user types (residential, industrial and commercial), P_{Ni} represents the rated power of node i, θ_{si} represents the proportion of load type s at node i, and δ_s represents the daily demand curve for load type s.

D. EVs

EVs' patterns of access to the power grid can be divided into two types: distributed and centralized. Among them, centralized access patterns for EVs can greatly improve the charge-discharge power rate [32], which has a great impact on the system power flow. Therefore, this paper considers a centralized pattern for EV access to the distribution system.

In the literature, research has shown that EVs are typically in a stopped state for more than 90% of the time [33], providing convenient opportunities for the flexible scheduling of power charging and discharging for EVs. The batteries of EVs are usually discharged during peak load times and charged during off-peak load times in the system to reduce the peak-valley difference. This article considers two kinds of charging/discharging strategies under different levels of EV penetration, where EV penetration is defined as the percentage of the system's rated capacity that is accounted for by the capacity of the EV access system.

1) Random charging pattern. Charging stations do not provide power service to the system but only charge batteries in accordance with their own needs.

2) Smart charging/discharging pattern. Each charging station adjusts its charging and discharging power in accordance with load demands and DG outputs to better suppress the peak-valley load difference for the distribution system. In this paper, it is assumed that the charging/discharging power rate in time period t obeys a normal distribution of mean $\mu_{v,t}$ and variance $\sigma^2_{v,t}$.

III. MATHEMATICAL DESCRIPTION OF THE PROBLEM

A. OBJECTIVE FUNCTION

In this paper, the goal of optimization is to minimize the active power loss, the load balancing index and the maximum node voltage deviation of the distribution network. The number of switching operations should also be minimized as much as possible in the proposed reconstruction model to ensure the economy and power quality of the system during operation.

1) POWER LOSS INDEX

Regarding the operation economy of the system, the total active power loss during hourly reconfiguration can be calculated according to the following formula:

$$f_1 = \min \sum_{T=1}^{TL} \sum_{m=1}^{M} D_m R_m \frac{P_m^2 + Q_m^2}{V_m^2} \tag{4}$$

where P_m, Q_m, R_m and V_m represent the active power, reactive power, resistance and initial voltage, respectively, of branch m; D_m is a binary value, where $D_m = 1$ and $D_m = 0$ represent the closed and open states, respectively, of the switch for branch m; M represents the total number of branches; and TL represents the time length.

2) LOAD BALANCING INDEX

Regarding the load balancing process, the total load balancing index during hourly reconfiguration can be calculated according to the following formula:

$$f_2 = \min \sum_{T=1}^{TL} \sum_{m=1}^{M} D_i \frac{\sqrt{P_m^2 + Q_m^2}}{S_m^{\max}} \tag{5}$$

where S_m^{max} represents the maximum complex power of branch m.

3) VOLTAGE DEVIATION INDEX

Regarding the voltage quality of the system during operation, the total voltage deviation index during hourly reconfiguration can be calculated according to the following formula:

$$f_3 = \min \sum_{T=1}^{TL} \max \left(\frac{V_1 - V_{1r}}{V_{1r}}, \cdots, \frac{V_i - V_{ir}}{V_{ir}}, \cdots, \frac{V_N - V_{Nr}}{V_{Nr}} \right) \tag{6}$$

where V_i and V_{ir} respectively represent the virtual and rated voltage of the node i, and N is the total number of nodes.

B. OPERATIONAL CONSTRAINTS

1) NETWORK POWER FLOW CONSTRAINT

$$\begin{cases} P_i + P_{DGi} - P_{Li} = V_i \sum_{j=1}^{N} U_j (G_{ij} \cos\theta_{ij} + B_{ij} \sin\theta_{ij}) \\ Q_i + Q_{DGi} - Q_{Li} = V_i \sum_{j=1}^{N} U_j (G_{ij} \sin\theta_{ij} - B_{ij} \cos\theta_{ij}) \end{cases} \tag{7}$$

where P_{DGi} represents the active power of the DG connected to the ith node.

2) NODE VOLTAGE CONSTRAINT

$$V_i^{\min} \le V_i \le V_i^{\max} \tag{8}$$

where V_i^{min} and V_i^{max} represent the given upper and lower voltage limits at node i, respectively.

3) BRANCH CAPACITY CONSTRAINT

$$S_k \le S_k^{\max} \tag{9}$$

where S_i^{max} is the upper capacity limit of branch k.

4) NETWORK TOPOLOGY CONSTRAINT

The distribution network maintains a radial structure, and there are no closed loops or isolated islands after its reconfiguration.

The PLR is a comprehensive index used to evaluate the operation economy and technical management of a power grid. The formula is expressed as

$$\lambda_{PLR} = P_l / (P_l + P_{total}) \tag{10}$$

where P_l represents the total active power loss and P_{total} represents the total load.

IV. DISTRIBUTION NETWORK RECONFIGURATION BASED ON THE LDBAS ALGORITHM

A. THE BEETLE ANTENNAE SEARCH (BAS) ALGORITHM

The BAS algorithm is a biologically inspired intelligent optimization algorithm that has a fast computing speed and a fast convergence rate for individual searches [34]. Each beetle flies through the problem space and is regarded as a potential solution to the problem. The position of a beetle is related to the intensity of the food odours it receives on its two antennae. The coordinate positions of the left and right antennae of the beetle are defined as

$$\begin{aligned} x_l^t &= x^t + d_0 \cdot \vec{d} \\ x_r^t &= x^t - d_0 \cdot \vec{d} \end{aligned} \tag{11}$$

where x_l^t and x_r^t represent the coordinate positions of the left and right antennae, respectively, in iteration number t; x^t is the position of the beetle in iteration number t; and d_0 represents the sensing diameter of the antennae. $\vec{d}$ represents a random vector.

$$\vec{d} = \frac{rands(n, 1)}{|rands(n, 1)|} \tag{12}$$

where $rands(n, 1)$ denotes the random number function and n denotes the number of spatial dimensions.

The intensity of the food odour is simulated in accordance with the fitness functions $f(x_l^t)$ and $f(x_r^t)$, and the next position of the beetle is updated as follows:

$$x^{t+1} = x^t - \delta^t \cdot \vec{d} \cdot sign(f(x_l^t) - f(x_r^t)) \tag{13}$$

where

$$\delta^t = \lambda \cdot \delta^{t-1} \tag{14}$$

$$d_0 = \delta^t / c \tag{15}$$

and δ^t denotes the step size; $sign(\cdot)$ is the sign function, λ denotes the rate of change in the step size δ, and c is the ratio between the step size δ and d_0.

B. LDBAS BASED ON LÉVY FLIGHT AND CHAOTIC DISTURBANCE

The BAS algorithm has a fast computation ability for individual searches. However, it is prone to premature convergence when solving high-dimensional multiobjective problems and thus tends to fall into local optima. Therefore, to address this shortcoming, the new LDBAS algorithm is proposed by introducing the Lévy flight strategy and chaotic disturbance in the search process.

1) LÉVY FLIGHT

Whether the BAS algorithm can find the optimal solution is closely related to the distance d between the two antennae of a beetle, the step length δ^t and the corresponding attenuation coefficient λ. The Lévy flight strategy is a search strategy for the BAS algorithm that represents foraging behaviour to improve convergence. Specifically, Lévy flight [35], [36] is a random search strategy in which the flight step follows a Lévy distribution with a heavy-tailed shape and can usually be obtained as follows:

$$\text{Lévy} \sim u = t^{-\beta}, \quad (1 < \beta \leq 3) \tag{16}$$

Moreover, the random vector $L(\beta)$ is calculated as

$$L(\beta) = \frac{\mu}{|v|^{\frac{1}{\beta}}} \tag{17}$$

where $\beta = 1 + \lambda$, $\lambda \in (0, 2]$, and μ and v follow normal distributions, $\mu \sim N(0,\phi^2)$ and $v \sim N(0, 1)$. In particular, $\beta = 1.5$ is used in this paper.

where

$$\phi = \left\{ \frac{\Gamma(1+\beta)\sin\left(\frac{\pi\beta}{2}\right)}{\beta\Gamma\left(\frac{1+\beta}{2}\right)2^{\frac{\beta-1}{2}}} \right\}^{\frac{1}{\beta}} \tag{18}$$

and $\Gamma(\cdot)$ is the standard gamma function.

Thus Equation (9) is updated to the following formula:

$$\begin{aligned} x_l^t &= x^t + 0.1^*\text{rand}(1)^*\text{L}(\beta) * \left|x^t - x_{best}\right| \\ x_r^t &= x^t - 0.1^*\text{rand}(1)^*\text{L}(\beta) * \left|x^t - x_{best}\right| \end{aligned} \tag{19}$$

2) CHAOTIC DISTURBANCE

Chaotic motion has the characteristics of randomness, ergodicity and regularity [37]. Chaotic disturbance is introduced into the LDBAS algorithm to prevent it from falling into local optima. Here, the search strategy of the BAS algorithm is implemented in accordance with the similarity defined by Equations (18), (19) and (20).

$$D(x_{worst}, x_j) = \frac{d(x_{worst}, x_j) - d_{\min}}{d_{\max} - d_{\min}}, \quad (d_{\min} < d(x_{worst}, x_j) < d_{\max}) \tag{20}$$

where x_{worst} represents the position of the beetle with the worst fitness value, $d(x_{worst}, x_j)$ represents the Euclidean distance between x_j and x_{worst}, and d_{min} represents the smallest distance.

The number of beetles affected by chaotic disturbance is

$$C = \sum_{j=1}^{N} c_j \tag{21}$$

$$c_j = \begin{cases} 1, & rc_i < D(x_{best}, x_j) \\ 0, & rc_i < D(x_{best}, x_j) \end{cases} \tag{22}$$

where N represents the number of individuals in the population and rc_i represents a random number between 0 and 1.

The logistic map is described as follows:

$$X_j^{C+1} = \sigma X_j^C (1 - X_j^C), \quad C > 0.2N \tag{23}$$

where σ represents the control parameter, $\sigma = 4$.

The position of each beetle is updated using the following formula:

$$x_{temx} = x_j^{\min} + X_j^{C+1}(x_j^{\max} - x_j^{\min}) \tag{24}$$

$$\begin{aligned} x_j^{C+1} = {} & r_{1j}{}^* x_j^C + (1 - r_{1j}) x_{best} + \delta(x_{temx} - x_j^C) \\ & {}^* sign(r_{2j} - 0.5)^*(-\log(r_{1j})) \end{aligned} \tag{25}$$

where $\boldsymbol{r_{1j}}$ and $\boldsymbol{r_{2j}}$ represent random numbers between 0 and 1.

3) TARGET DECISION-MAKING METHOD

Grey target decision theory is generally used to sort, grade and select evaluation schemes [38]–[40]. Here, the grey target decision-making method is implemented to determine the most satisfactory topology based on multiple conflicting indexes.

A set of possible reconfiguration schemes is defined as s_i, $i = 1, 2, \cdots, m$, which are obtained using the LDBAS method. We also define a distribution network reconfiguration index as $j \in n = \{1, 2, 3\}$. Thus, s_{ij} denotes the effect value of reconfiguration scheme s_i corresponding to index j, and the sample effect matrix is $S = [s_{ij}]_{m\times 3}$.

Then, the decision matrix $R = [r_{ij}]_{n\times m}$ can be described as

$$r_{ij} = \frac{\min\limits_{1\leq i\leq m} s_{ij}}{s_{ij}} \tag{26}$$

Equation (24) is a cost index because the indexes used to measure the performance of the distribution network are all cost objective functions in this study.

$$\chi\left(r_{i0}, r_{ij}\right) = \frac{\min\limits_{1\leq i\leq m}\min\limits_{1\leq j\leq 3}\Delta_i(0,j) + \rho\max\limits_{1\leq i\leq m}\max\limits_{1\leq j\leq 3}\Delta_i(0,j)}{\Delta_i(0,j) + \rho\max\limits_{1\leq i\leq m}\max\limits_{1\leq j\leq 3}\Delta_i(0,j)} \tag{27}$$

$$\chi\left(r(0), r(j)\right) = \frac{1}{m}\sum_{i=1}^{m}\chi\left(r_{i0}, r_{ij}\right) \tag{28}$$

$$w_j = \frac{\chi\left(r(0), r(j)\right)}{\sum\limits_{r=1}^{3}\chi\left(r(0), r(j)\right)} \tag{29}$$

where $\chi(r_{i0}, r_{ij})$ represents the contribution coefficient of index j to the reconfiguration solution s_i, $\Delta_i(0, j) = |r_{i0} - r_{ij}|$,

$\rho = 0.5$, $\chi(r_0, r_j)$ represents the contribution of index j, and w_j represents the weight of index j.

In addition, we define the ideal solution s^0 (namely, the target centre) corresponding to the decision vector $r^0 = \{r_1^0, r_2^0, r_3^0$, where $r_j^0 = \max\{r_{ij} \mid 1 \le i \le m\}$, $j = 1, 2, 3$.

With this definition of grey target decision-making, the distance from a solution s_i to the ideal solution s_0 is denoted by DD_i; in other words, DD_i is the target centre distance. The smaller DD_i is, the more satisfactory solution s_i is.

$$DD_i = \left| r_i - r^0 \right| = \sqrt{\sum_{j=1}^{3} \omega_j (r_{ij} - r_j^0)^2} \tag{30}$$

C. LDBAS ALGORITHM

In this study, the LDBAS algorithm is proposed to obtain the most satisfactory solution for the reconfiguration of the distribution network. For a reconfiguration model with multiple objective functions, a grey target decision-making method is introduced to sort the beetles. First, initial models of 'pbest' are randomly generated in the search space, and the generated beetle individuals are ranked via the grey target decision-making method. To improve the diversity of the beetle population, (1) the beetles are selected based on the similarity obtained using chaotic sequences, and (2) the search behaviour of the other beetles is updated using the Lévy flight strategy. Finally, the fitness values of the updated beetle individuals are calculated and ranked again. Table 1 presents the general procedure of the LDBAS method.

TABLE 1. LDBAS algorithm flow.

Algorithm 1 LDBAS algorithm
Input: System parameters, loads and DG, index constraints, and LDBAS algorithm.
Output: the optimal switch combination.
1: Generate 'pbest' beetles to be the initial population number randomly.
2: **tic**
3: Evaluate the indexes for these initial beetles.
4: Sort the beetles by using grey target decision-making technique, the best solution 'gbest' is retained by (30)
5: While termination criterion not fulfilled do
6: Update the left and right antennae using Eq. (13), ggbest=fitnessfunction(gbest);
7: **for** k=1: pbest do
8: **If** k== 1 {F = sort(gbest); OF=sort(ggbest);} **Else** {F= sort (M_{k-1}, M); OF= sort (OM_{k-1}, OM);} **end if**
9: Update the left and right antennae using Eq. (11)
10: Chaotic disturbance mechanism is carried out for the beetles by using similarity theory, according to the given formula: $C = \sum_{j=1}^{n} c_j$.
11: for each beetle
12: {Update the position of the current beetle using Lévy flight (Eq. (19))};**end for**
13: Rank the beetles by using grey target decision-making technique, and the best beetle 'gbest' is retained as a basic solution for chaotic disturbance mechanism and Lévy flight end for
14: **end while**
15: Return 'gbest' and corresponding results of each index.

D. APPLICATION OF THE LDBAS ALGORITHM TO THE RECONFIGURATION PROBLEM

1) CODING PATTERN BASED ON A BASIC LOOP

In this study, a method of encoding particles with decimal integers based on a loop topology is adopted, and the number of contact switches is taken as the particle dimension. A switch is selected in each loop to be opened to form a new topological solution, as shown in the following formula:

$$x = [x_{e1}, x_{e2}, \cdots, x_{ei}, \cdots, x_{el}] \tag{31}$$

where x_{ei} represents the number of open switches in loop i.

The modified IEEE 33-node distribution system in Fig. 1 is taken as an example; it contains 33 nodes, 32 branches, and 5 tie switches. The loop matrix M forms the simplified topology of Fig. 1 and is expressed as shown in (30).

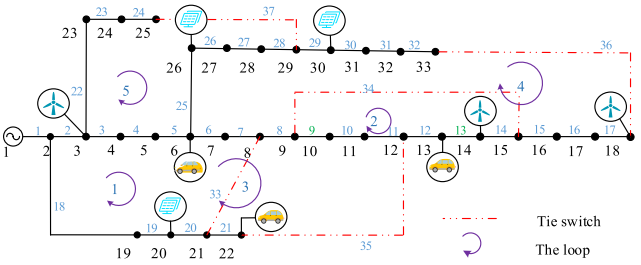

FIGURE 1. Modified IEEE 33-node distribution system.

The proposed reconfiguration method defines processes for network reconfiguration under two kinds of operating modes: OR can be performed by calculating the predicted loads and the DG power levels for the next day, and RTR can be performed for a 1-hour interval calculated via power forecasting over a 1-hour time horizon. The PLR for the 1-hour reconfiguration is compared with that for the OR solution. The optimal solutions for reconfiguration in both operation modes can be found by using the proposed algorithm. The flowchart of the proposed algorithm is shown in Fig. 2.

2) SOLUTION PROCESS FOR THE DYNAMIC RECONSTRUCTION OF A DISTRIBUTION NETWORK

From the mathematical model for the dynamic reconstruction of the distribution network, it can be seen that two main difficulties arise when solving the optimization problem for dynamic reconstruction. (1) The optimization for a single period (a certain time segment) exhibits spatial complexity. (2) The optimization for the whole time duration exhibits temporal complexity.

To address the above problem, this paper proposes a dynamic reconfiguration method based on the PLR that can be divided into three steps. First, a day is divided into 24 periods with a time interval of $\Delta t = 1\ h$; the topological solution for the OR mode for the whole day and the RTR solutions for all 24 periods are obtained via the LDBAS method, and the PLRs for the two reconfiguration modes are calculated according to formula (10). Second, the PLR

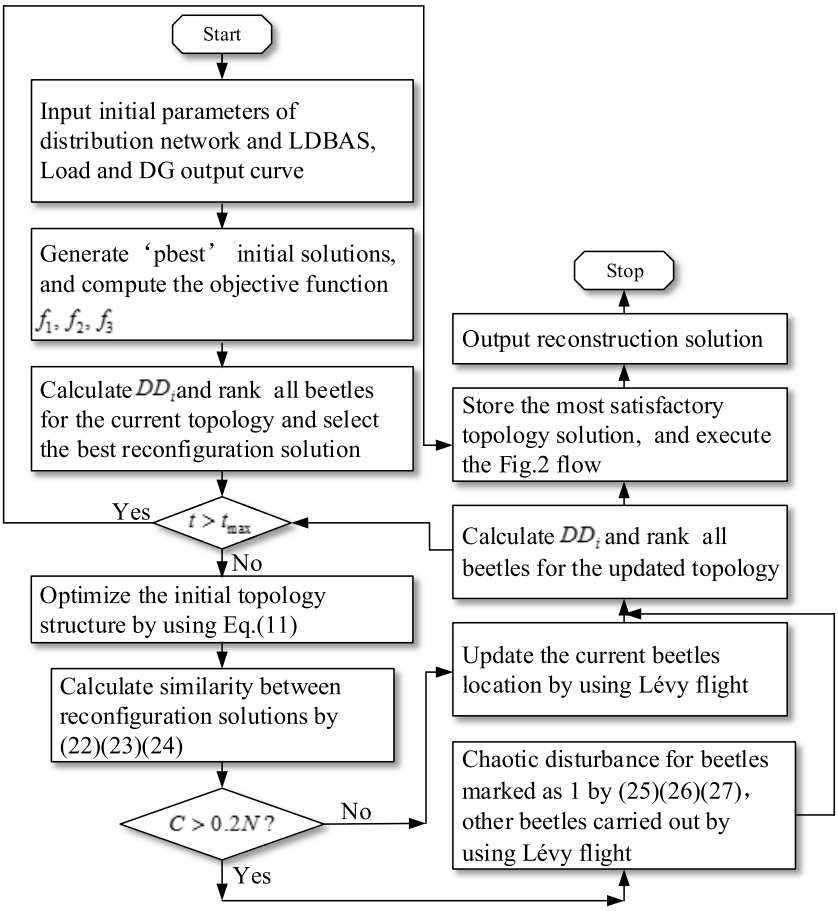

FIGURE 2. Flow chart of distribution network reconfiguration based on the LDBAS algorithm.

reduction curve for the day is obtained via (33). Furthermore, the PLR reduction value for each pair of adjacent time periods is considered in turn, and if it exceeds a given threshold λ_g, then the topological solution for the RTR mode in the corresponding period is stored in the external solution set $S_{T_K}(i)$. Third, the optimal topological solution for $S_{T_K}(i)$ is found using the grey target decision-making technique. Fig. 3 shows the flow chart of the proposed dynamic reconfiguration model.

$$\Delta\lambda_s = \left|\lambda_{op}(T_k) - \lambda_{rt}(T_k)\right| \tag{33}$$

where $\Delta\lambda_s$ represents the PLR reduction value between the two reconfiguration modes in time period T_k, $\lambda_{op}(T_k)$ represents the PLR for the OR mode, and $\lambda_{rt}(T_k)$ represents the PLR for the RTR mode.

V. NUMERICAL SIMULATION

A. PARAMETER SETTINGS

To verify the effectiveness of the proposed algorithm, seven benchmark test functions, as shown in Table 2, are selected as the objective function to perform simulation tests on LDBAS, and two basic algorithms, BAS and chaotic disturbance BAS (CDBAS), are tested to compare the performance of each algorithm. Meanwhile, to compare the convergence speed and accuracy and the global search ability of each algorithm more clearly and accurately, each algorithm is run independently 50 times. The Sphere, Rosenbrock and Step functions are typical unimodal functions. The dimension D of each test function is set as 5, 30 and 50, and the algorithm parameters are set as $t_{max} = 1000$, $\lambda = 0.95$, $c = 5$, and $\delta = 1$. The test functions and their parameter settings are shown

$$M = \begin{bmatrix} 7 & 6 & 5 & 4 & 3 & 2 & 20 & 19 & 18 & 33 & 0 & 0 & 0 & 0 & 0 & 0 & 0 & 0 & 0 & 0 \\ 14 & 13 & 12 & 11 & 10 & 9 & 34 & 0 & 0 & 0 & 0 & 0 & 0 & 0 & 0 & 0 & 0 & 0 & 0 & 0 \\ 11 & 10 & 9 & 8 & 7 & 6 & 5 & 4 & 3 & 2 & 21 & 20 & 19 & 18 & 35 & 0 & 0 & 0 & 0 & 0 \\ 17 & 16 & 15 & 14 & 13 & 12 & 11 & 10 & 9 & 8 & 7 & 6 & 32 & 31 & 30 & 29 & 28 & 27 & 26 & 25 \\ 24 & 23 & 22 & 28 & 27 & 26 & 25 & 5 & 4 & 3 & 37 & 0 & 0 & 0 & 0 & 0 & 0 & 0 & 0 & 0 \end{bmatrix} \tag{32}$$

TABLE 2. Benchmark test functions.

Name	Function	Dim	Range	g_{min}
Sphere	$g_1(x)=\sum_{i=1}^{d} x_i^2$	5	[-10, 10]	0
Rosenbrock	$g_2(x)=\sum_{i=1}^{d-1}\left[100\left(x_{i+1}-x_i^2\right)^2+\left(x_i-1\right)^2\right]$	5	[-10, 10]	0
Step	$g_3(x)=\sum_{i=1}^{D}\left[x_i+0.5\right]^2$	5	[-10, 10]	0
Ackley	$g_4(x)=-20\exp[-0.2\sqrt{\frac{1}{d}\sum_{i=1}^{d}x_i^2}]-\exp\left[\frac{1}{d}\sum_{i=1}^{d}\cos\left(2\pi x_i\right)\right]$	5	[-10, 10]	0
Rastrigin	$g_5(x)=10d+\sum_{i=1}^{d}\left[x_i^2-10\cos\left(2\pi x_i\right)\right]$	5	[-10, 10]	0
Dixon-Price	$g_6(x)=\left(x_1-1\right)^2+\sum_{i=2}^{d} i\left(2x_i^2-x_{i-1}\right)^2$	5	[-10,10]	0
Michalewicz	$g_7(x)=-\sum_{i=1}^{d}\sin\left(x_i\right)\sin^{2m}\left(\frac{ix_i^2}{\pi}\right)$	5	[0, π]	-4.68766

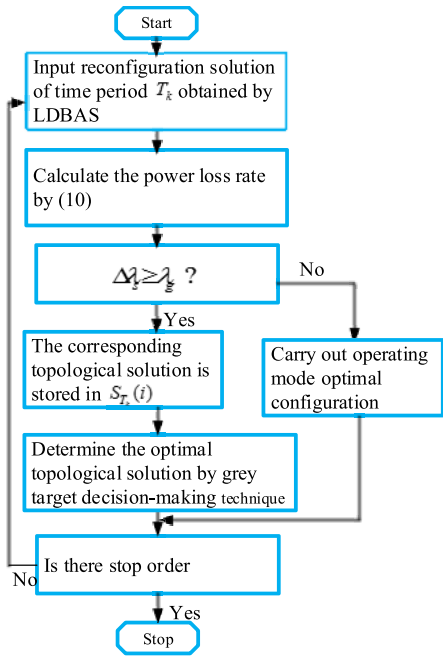

FIGURE 3. Flowchart of the proposed dynamic reconfiguration model.

in Table A.1 of Appendix A. The software environment in which this study was implemented is by Intel(R) Core(TM)i5-5200U 2.20GHz CPU 4GB RAM and Matlab2014a.

B. SIMULATION RESULT

To compare the optimization capabilities of each algorithm more intuitively, Tables 3, 4 and 5 give the average, optimal, and worst values and the average value and square difference for 5D, 30D and 50D.

Fig. 4 shows the optimization process of the seven test functions with the same parameters for each algorithm. We find that LDBAS and CDBAS, compared with the BAS algorithm, show absolute superiority in escaping local optima and in terms of optimization accuracy, and the optimal solution is obtained within the first few steps of the iteration. In the comparison of these two algorithms, the optimization result of LDBAS for the Michalewicz function is significantly better than that of CDBAS, and the LDBAS algorithm optimization is slightly more accurate for the other six test functions, which also shows that the Lévy flight can better drive the BAS algorithm to search for the optimal solution.

It can be seen from Tables 3, 4 and 5 that the optimization results of the LDBAS algorithm for the selected test functions are best compared with the CDBAS and BAS algorithms in 5D. On the other hand, as the search dimensionality increases, LDBAS can still iterate to the vicinity of the optimal value, while the BAS algorithm has difficulty achieving the optimal value and cannot adapt to the optimization of high-dimensional functions. Thus, the modified BAS algorithm can enhance the accuracy, stability and global search ability of the original BAS algorithm.

VI. RESULTS

In this study, the modified IEEE 33-node system and the modified IEEE 118-node system are taken as examples. The proposed method is used to find the optimal solution for the dynamic reconfiguration of the distribution network, with the population size in the LDBAS algorithm set to

TABLE 3. Performance comparison of seven functions when the search dimension is 5D.

Function	Algorithm	Min	Max	Mean	Std
g1	BAS	1.30×10^{-9}	36.5103	1.6275	5.4057
	CDBAS	1.94×10^{-10}	22.8490	0.1273	1.6132
	LDBAS	3.52×10^{-8}	7.2707	0.1064	0.6573
g2	BAS	3.054738	50365.6099	1504.0233	6900.2231
	CDBAS	0.049875	6479.8221	36.1498	457.3262
	LDBAS	0.105196	5496.3339	96.8157	571.9514
g3	BAS	8.84×10^{-10}	22.1522	1.2590	4.0735
	CDBAS	1.87×10^{-10}	30.5588	0.2443	2.2412
	LDBAS	2.03×10^{-8}	10.7820	0.2414	1.3452
g4	BAS	5.16271	9.2080	5.7048	0.8917
	CDBAS	3.27×10^{-5}	10.1986	0.2683	1.0320
	LDBAS	0.00023	6.4682	0.3125	1.0610
g5	BAS	11.9395	69.8399	17.3201	10.8634
	CDBAS	3.97984	78.6086	5.7094	6.2558
	LDBAS	0.99496	63.5167	3.1623	7.7927
g6	BAS	1.23544	2163.8888	51.5196	241.5353
	CDBAS	3.41×10^{-7}	1028.4140	5.5865	72.5856
	LDBAS	4.63×10^{-5}	1485.8136	24.4253	155.8497
g7	BAS	-3.5736	-1.9462	-3.4745	0.1753
	CDBAS	-3.8616	-2.0097	-3.7339	0.2549
	LDBAS	-4.6877	-2.2816	-4.6132	0.3726

TABLE 4. Performance comparison of seven functions when the search dimension is 30D.

Function	Algorithm	Min	Max	Mean	Std
g1	BAS	467.5628	594.0950	480.5830	26.4957
	CDBAS	7.699121	621.2890	14.2977	43.8090
	LDBAS	3.78×10^{-5}	524.2940	54.8696	140.5137
g2	BAS	1606409	2657565	1701215	204599
	CDBAS	909.2336	2973569	16815	209630
	LDBAS	29.1382	2285222	165877	489937
g3	BAS	524.1083	667.4628	537.6663	28.3730
	CDBAS	2.0654	635.5627	8.3597	45.6157
	LDBAS	3.38×10^{-5}	696.7462	57.5041	162.1706
g4	BAS	12.7100	13.8161	12.9032	0.2961
	CDBAS	3.4891	13.6815	3.7906	0.8764
	LDBAS	2.2210	14.0465	3.7597	3.1881
g5	BAS	650.2599	921.7691	678.0965	48.9841
	CDBAS	66.7249	894.5821	103.2769	77.0625
	LDBAS	35.8209	943.6601	114.5368	203.3442
g6	BAS	542174.64	821138.15	573627.36	62001.61
	CDBAS	173.21	1718348.26	9257.30	121178.02
	LDBAS	0.6945	1705533.23	145872.57	419453.94
g7	BAS	-13.7004	-6.6893	-11.5006	2.4023
	CDBAS	-14.2375	-6.7658	-12.5964	1.7335
	LDBAS	-15.8714	-7.2879	-13.5152	1.8411

300 and the maximum number of iterations set to 1000. To observe the differences in the influence of EVs on the load curve, active power loss and voltage of the distribution network under different EV penetration rates and the two different charging/discharging patterns, seven different scenarios are assumed, as follows: scenario 1, without EVs; scenario 2, with an EV penetration rate of 0.25 under the random charging pattern; scenario 3, with an EV penetration

TABLE 5. Performance comparison of seven functions when the search dimension is 50D.

Function	Algorithm	Min	Max	Mean	Std
g1	BAS	1131.20	1284.78	1146.69	30.84
	CDBAS	55.1987	1088.1862	67.4591	74.1254
	LDBAS	0.0174	1179.3254	180.4864	319.7112
g2	BAS	4107425.57	5605010.31	4237142.29	273388.34
	CDBAS	15845.60	6325968.81	51600.34	444943.66
	LDBAS	49.16	6309898.63	518911.62	1490937.51
g3	BAS	936.02	1075.42	949.86	29.08
	CDBAS	40.3170	1211.9779	52.9710	83.8998
	LDBAS	0.0001	1268.7462	106.2769	310.8050
g4	BAS	12.4956	13.1698	12.6143	0.1895
	CDBAS	5.7205	14.0828	5.9662	0.6756
	LDBAS	3.5748	14.3222	4.9538	2.9983
g5	BAS	1401.49	1645.53	1437.87	61.46
	CDBAS	238.23	1730.90	290.38	124.40
	LDBAS	40.8403	1413.2760	234.8190	391.4864
g6	BAS	3853589.60	5385809.18	3983584.11	277162.64
	CDBAS	764.99	5835757.58	31277.95	411558.47
	LDBAS	0.8312	5562420.40	472073.40	1442801.98
g7	BAS	-17.8182	-9.6395	-15.2049	2.5751
	CDBAS	-22.6369	-9.8585	-19.7598	2.9509
	LDBAS	-22.8548	-9.4998	-21.4042	2.8323

rate of 0.5 under the smart charging/discharging pattern; scenario 4, with an EV penetration rate of 0.9 under the random charging pattern; scenario 5, with an EV penetration rate of 0.25 under the smart charging/discharging pattern; scenario 6, with an EV penetration rate of 0.5 under the random charging pattern; and scenario 7, with an EV penetration rate of 0.8 under the smart charging/discharging pattern. Moreover, the above seven scenarios are verified and analysed in distribution systems with DG.

1) Random charging strategy for EVs. It is assume that the EVs are charged at the average speed while they are driving and at the maximum charging power immediately after stopping. A random charging load is simulated for each charging station using the Monte Carlo method. Fig. 5 shows the charging load curve for 500 EVs.

2) Smart charging/discharging strategy for EVs. The mean power injected into the distribution system in each period is shown in Table 3, and the mean square deviation is 5% of the mean power.

The prediction parameters and the specific parameters and locations for DG and EV access to the distribution system are shown in Tables 6 and 7, respectively. Fig. 6 shows the Total equivalent loads under different charging/discharging strategies.

A. IEEE 33-BUS SYSTEM

In normal circumstances, the initial topology of the 33-bus system is as given in Fig. 3 [41]. The detailed system data consist of the daily load ratio for each node in the IEEE 33-bus system, as provided in [42]. The open branches in the original topology of the IEEE 33-bus network are 33, 34, 35, 36 and 37. Here, we set the upper and lower voltage limits to 0.9 p.u. and 1.05 p.u., respectively.

1) VALIDATION OF THE LDBAS ALGORITHM

To verify the effectiveness of the LDBAS algorithm for solving the distribution network reconfiguration problem, the IEEE 33-bus system is used for testing in scenario 1, and the BAS algorithm, the chaos disturbed beetle antennae search (CDBAS) algorithm, the PSO algorithm and a genetic algorithm (GA) are compared in accordance with the simulated OR results over 24 hours.

a: GLOBAL SEARCH ABILITY

Table 8 shows the optimal solutions obtained with the different algorithms. From the results for fitness value 2 in Table 4, it is clear that the solutions found by the LDBAS and CDBAS algorithms are both optimal, in contrast to the BAS, PSO, and GA solutions, because the Lévy flight strategy and chaotic disturbance effectively enhance the population diversity, making it easier for these algorithms to escape from local optima. Fitness value 1 is calculated for the optimal solution found by each algorithm, and fitness value 2 is calculated to sort the optimal solutions of the five algorithms by using the grey target decision-making method again. Fitness value 1 is different for the CDBAS and LDBAS algorithms, with values of 0.00843 and 0.00857, respectively. This is because the candidate individuals, the number of candidates or both are different when the candidate solutions are sorted via the grey target decision-making method.

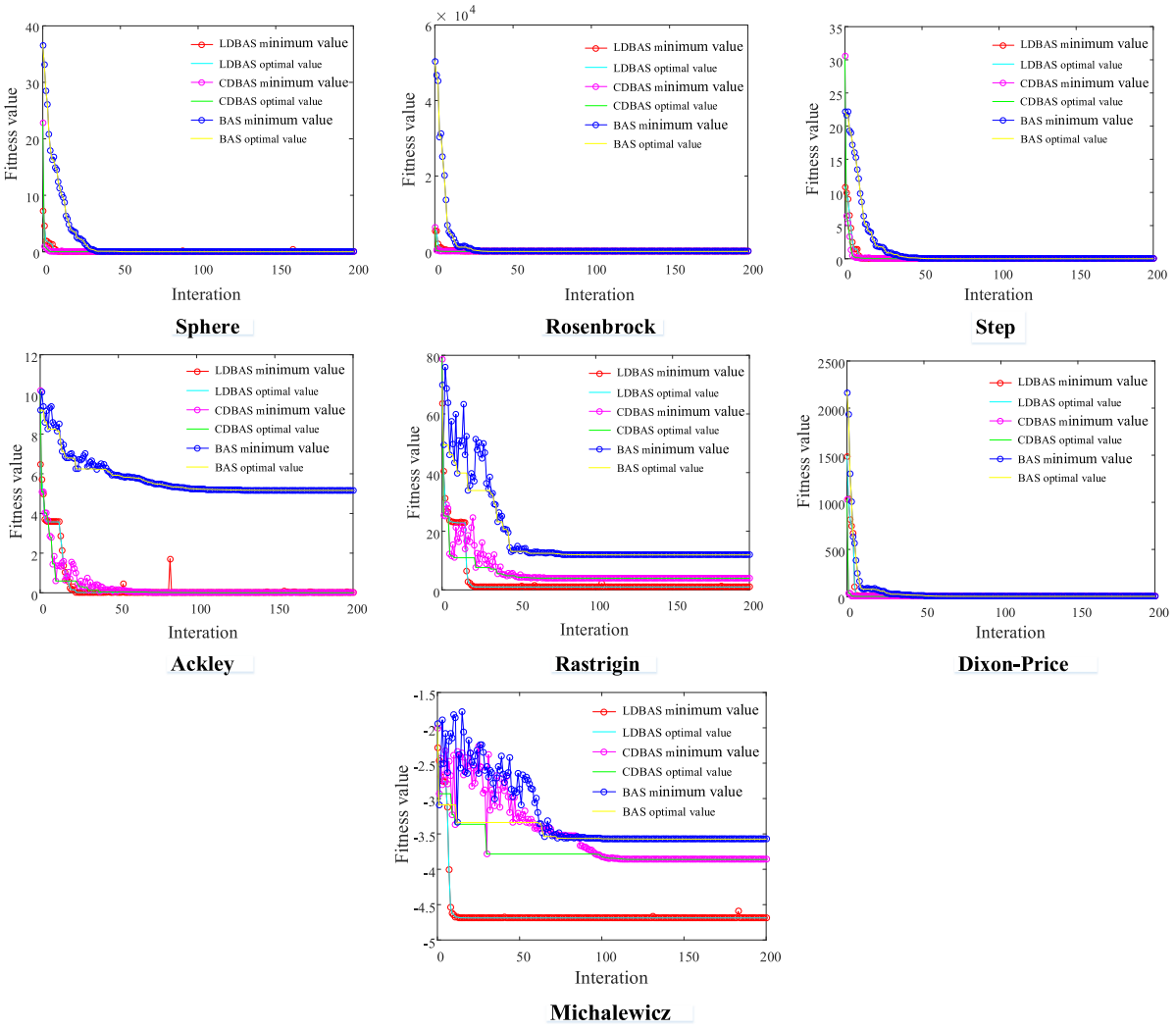

FIGURE 4. Evolutionary progress of objective function values for each algorithm.

TABLE 6. Prediction parameters for DG units and EVS in each period.

Hours	1	2	3	4	5	6	7	8	9	10	11	12
Mean values of wind speed (m/s)	14.2	17.4	10.5	7.9	8.1	9.5	9.2	8.7	9.3	5.4	6.2	7.8
Maximum values of solar radiation (W/m^2)	0	0	0	0	0	0	10	49.8	136	174.5	223.9	292.9
Power injected by EV charging station (MW)	-0.695	-0.657	-0.709	-0.731	-0.402	-0.519	-0.23	0	0	0.118	0.138	0
Hours	13	14	15	16	17	18	19	20	21	22	23	24
Mean values of wind speed (m/s)	6.5	7.4	8.3	4.7	8.7	10.9	9.1	13.7	12.1	9.6	13.9	12.2
Maximum values of solar radiation (W/m^2)	0	0	0	0	0	0	10	49.8	136	174.5	223.9	292.9
Power injected by EV charging station (MW)	0	0	0	0.663	0.415	0.199	0.19	0.43	0.367	0	-0.06	-0.477

From the results for the active power loss and maximum node voltage deviation in Table 8, it is clear that the results of the LDBAS algorithm are slightly better than those of the PSO algorithm, but the PSO algorithm is slightly better in terms of the load balancing index. In other words, the proposed multiobjective reconfiguration method can consider both the economy and stability of system operation.

b: CONVERGENCE PERFORMANCE

From the results in Fig. 7, it is clear that the number of the convergence for each algorithm is 42, 15, 8, 129 and 38 times. Compared with CDBAS, BAS, PSO and GA algorithm, the result of fitness value for LDBAS algorithm is the optimal, although it does not have the least number of iterations.

TABLE 7. Specific parameters and locations for DG and EV access to IEEE 33- and 118-bus system.

Type	Location		Capacity (MW)	Speed parameters (m/s)	Photovoltaic panels parameters	Power factor
	33 bus	118 bus				
Wind turbine	7	48,71,106	1	$v_{ci}=4, v_r=14, v_{co}=24$		0.95
Photovoltaic panels	14	22			$A=13\,750(m^2), \eta=15\%$	0.95
EV	24	19,42,52,65 ,68,75,90, 98	Battery capacity 24 (kWh)	Energy consumption of battery 0.12 (kWh/km)	Maximum charge / discharge power 4(kW)	Battery efficiency 75%

TABLE 8. Results of different algorithms.

Algorithm	Open switches	Active power loss (kWh)	Load balancing index (p.u)	Maximum node voltage deviation (p.u)	Fitness value1	Fitness value 2
LDBAS	7 14 10 17 28	574.7680	2.2552	0.5004	0.00843	0.0083
CDBAS	7 14 10 17 28	574.7680	2.2552	0.5004	0.00857	0.0083
BAS	7 13 9 17 28	581.2183	2.2643	0.5048	0.01304	0.0139
PSO	7 14 9 32 28	583.6783	2.2498	0.5111	0.01465	0.016
GA	7 12 9 17 28	586.7605	2.2569	0.5436	0.01317	0.0467

TABLE 9. Results of different algorithms.

Algorithm	The average value of objective function	The running numbers	The average convergence times	The average time/s
LDBAS	0.00823	30	57.0666	748.04
CDBAS	0.00992	24	98.8400	852.78
BAS	0.02254	13	82.6251	824.86
PSO	0.02562	6	0.5111	1011.26
GA	0.02774	4	0.5436	1173.69

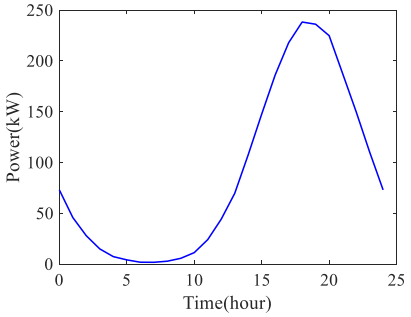

FIGURE 5. Charging load curve for 500 EVs obtained through Monte Carlo simulation.

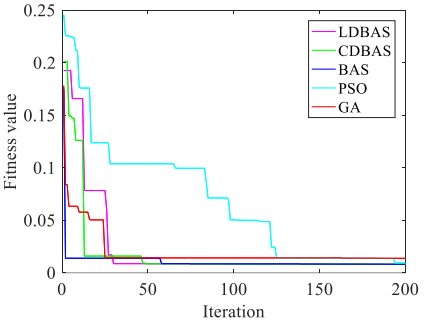

FIGURE 7. Comparison of the convergence behaviour of different algorithms.

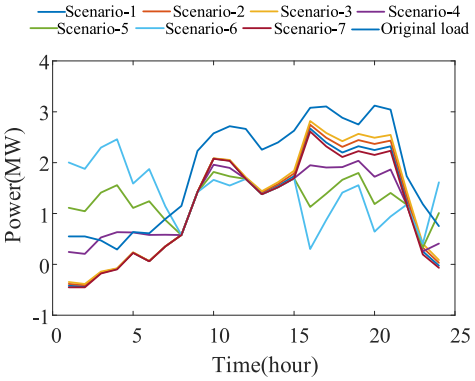

FIGURE 6. Total equivalent loads under different charging/discharging strategies.

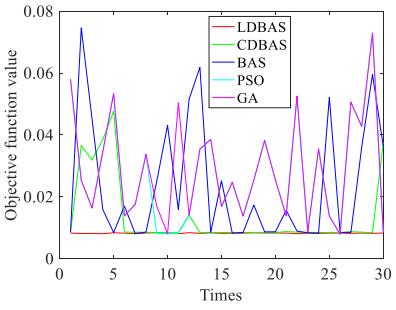

FIGURE 8. The optimal solutions found by different algorithms in 30 independent runs.

c: STABILITY

To illustrate the randomness of the intelligent algorithms, Fig. 8 shows the optimal solution curves for the LDBAS algorithm, the CDBAS algorithm, the BAS algorithm, the PSO algorithm and the GA in 30 independent runs.

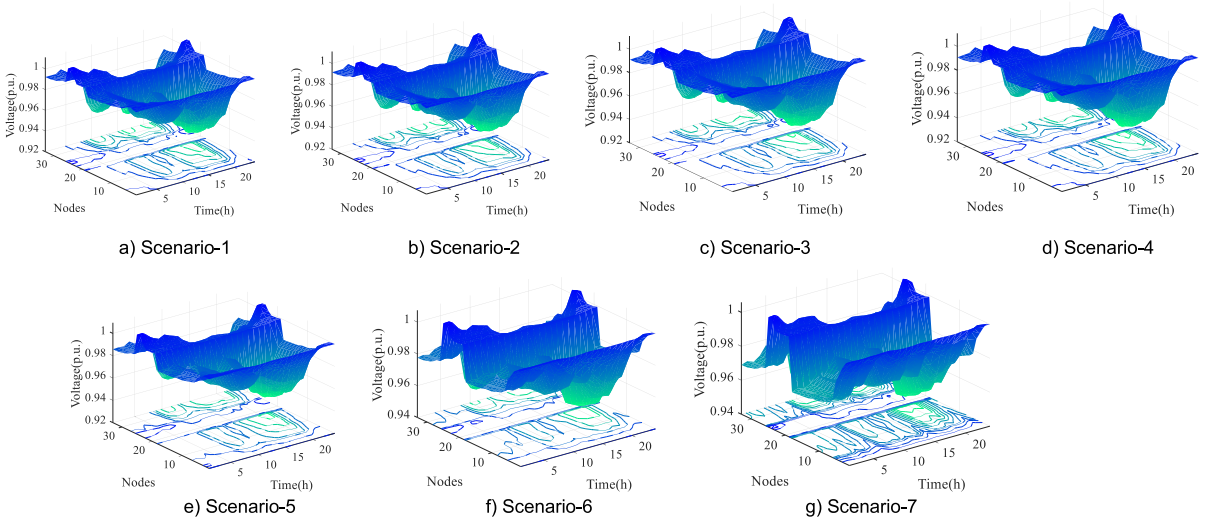

FIGURE 9. Voltage profiles of the 33-bus network with DG over 24 hours under different levels of EV penetration.

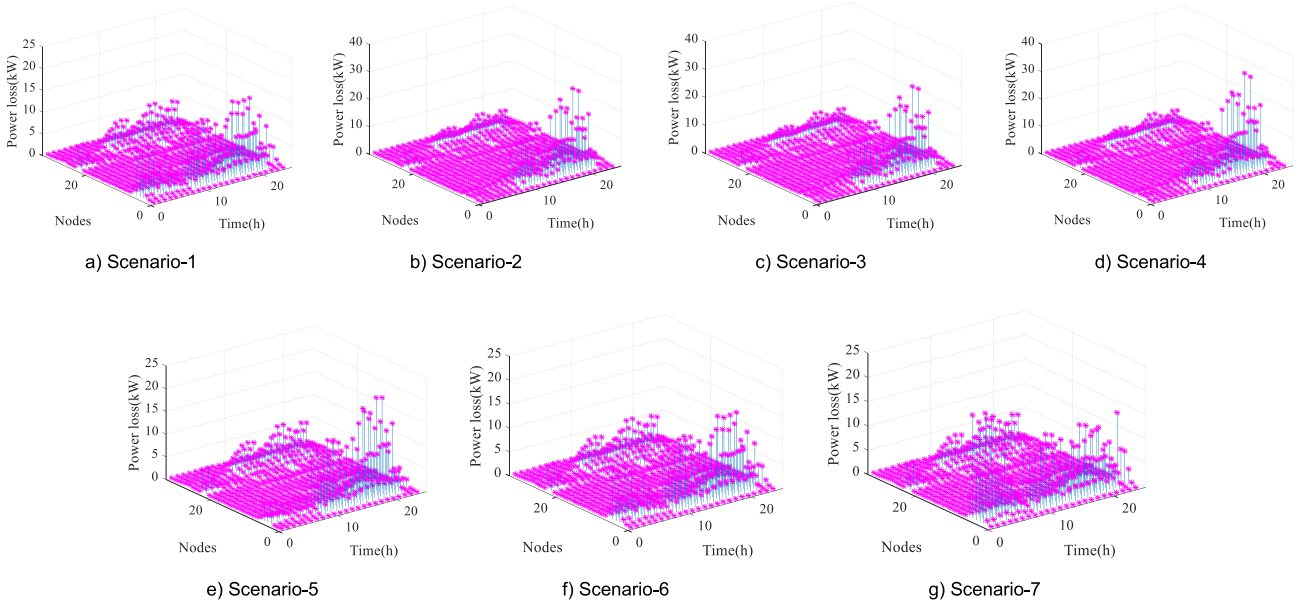

FIGURE 10. Power loss profiles of the 33-bus network with DG over 24 hours under different levels of EV penetration.

From the results in Table 9, it is clear that the average value of the objective function, the number of optimal solutions, the average convergence times and the average time of the LDBAS algorithm are better than those of the other four algorithms; in particular, its search efficiency is 100% according to the number of optimal solutions, much higher than the search efficiency of the other algorithms. In addition, from the results of Fig. 8, it is clear that the LDBAS algorithm shows better stability than the PSO algorithm and the GA, with negligible fluctuations.

2) INFLUNCE OF DIFFERENT EV PENETRATION FOR A DISTRIBUTION SYSTEM WITH DG

At different levels of penetration, EVs will affect the operation of the distribution system to different degrees. To investigate this influence, seven pre-set scenarios are simulated in the original system. Fig. 9 shows the voltage profiles of the 33-bus network with DG over 24 hours under different levels of EV penetration. In terms of the overall voltage profiles, we can clearly see that the voltage of the distribution network with EVs under the random charging pattern is decreased compared to scenario 1 without EVs, and the voltage drop becomes more severe as the penetration of EVs increases. However, compared with scenarios 1, 2, 3 and 4, the voltage of the network is improved under the smart EV charging/discharging pattern, as in scenarios 5, 6 and 7. From a local perspective on the voltage profile, the minimum voltage magnitudes in scenarios 1-7 are 0.9322 p.u. for node 20 at 18:00, 0.9307 p.u. for node 20 at 18:00, 0.9287 p.u. for node 20 at 18:00, 0.9267 p.u. for node 20 at 18:00, 0.9369 p.u.

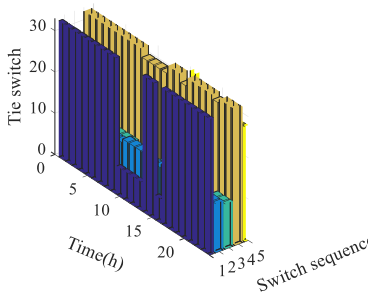

a) Distribution system with an EV penetration rate of 0.25

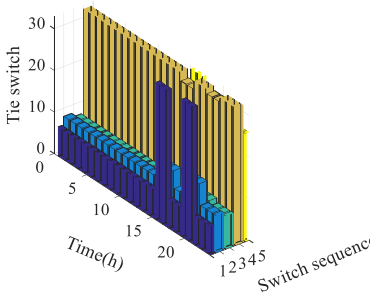

b) Distribution system with an EV penetration rate of 0.5

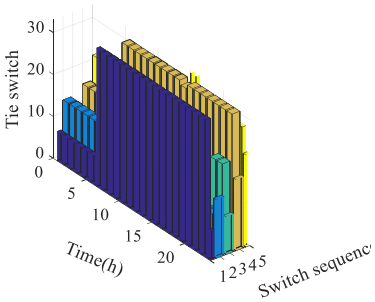

c) Distribution system with an EV penetration rate of 0.9

FIGURE 11. Switch states over 24 hours as determined with the proposed reconfiguration model under the smart charging/discharging pattern.

for node 20 at 18:00, 0.9422 p.u. for node 21 at 18:00, and 0.9471 p.u. for node 19 at 18:00, respectively. As the EV penetration rate increases, the minimum voltage value in the network rises significantly.

Fig. 10 shows the power loss profiles of the 33-bus network with DG over 24 hours under different levels of EV penetration. Regarding the overall power loss profile, the total active power losses in scenarios 1-7 are 1077.6122 kWh, 1114.1086 kWh, 1162.5720 kWh, 1214.8684 kWh, 1030.1023 kWh, 1045.6433 kWh, and 1143.4600 kWh, respectively. In other words, compared with the total active power losses of the network without EVs and with the smart EV charging/discharging pattern, the total active power losses under the random charging pattern, as in scenarios 1, 2, 3 and 4, are increased. On the other hand, the total power loss of the system in scenario 7 is increased by 6.11% compared to that in scenario 1. Thus, EV access to the 33-bus distribution network will initially reduce the network loss under the smart charging/discharging pattern,

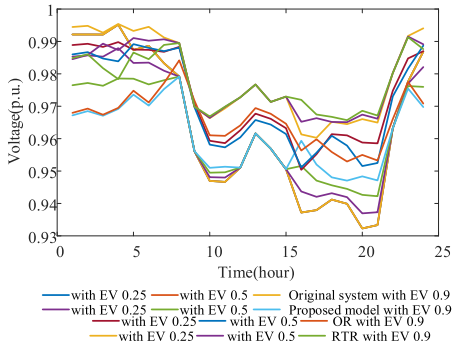

a) Minimum voltage profile

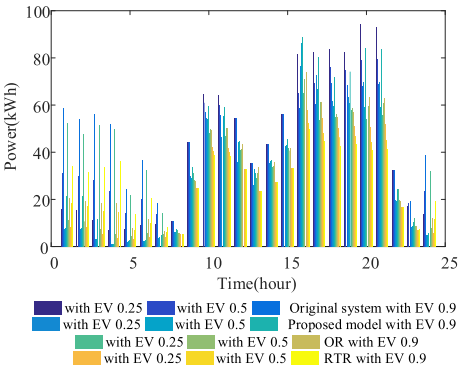

b) Total power loss profile

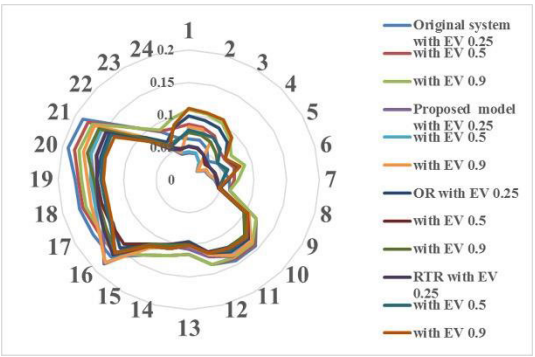

c) Total load balancing index

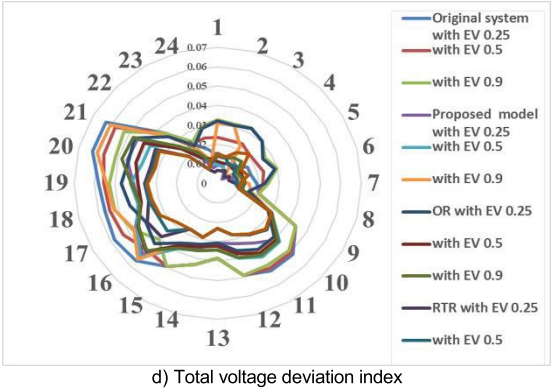

d) Total voltage deviation index

FIGURE 12. Results of the proposed reconfiguration method for the 33-bus network over 24 hours.

but when the EV penetration reaches a certain upper limit, it will increase the total power loss of the system.

TABLE 10. Actual operation mode with the proposed reconfiguration method for the 33-bus system under the smart charging/discharging.

Hour	OR mode with EV penetration 0.5		RTR mode with EV penetration 0.25		OR mode with EV penetration 0.5		RTR mode with EV penetration 0.5		OR mode with EV penetration 0.9		RTR mode with EV penetration 0.9	
	Power Loss (kW)	/PLR	Power Loss (kW)	/PLR	Power Loss (kW)	/PLR	Power Loss (kW)	/PLR	Power Loss (kW)	/PLR	Power Loss (kW)	/PLR
1	11.0419	0.0108	8.3594	0.0082	20.6471	0.0128	18.6733	0.0116	52.2278	0.0233	34.3072	0.0155
2	10.6792	0.0107	8.0918	0.0081	19.3771	0.0124	17.1777	0.0110	47.8464	0.0223	31.6652	0.0148
3	7.6185	0.0080	5.2586	0.0055	18.6656	0.0120	15.2335	0.0099	51.4078	0.0237	33.5255	0.0156
4	5.3336	0.0068	3.6882	0.0047	18.5473	0.0131	14.6652	0.0104	49.7099	0.0243	36.2088	0.0178
5	4.6532	0.0051	3.1273	0.0034	7.9275	0.0064	6.9996	0.0057	21.7007	0.0139	13.7435	0.0088
6	5.7547	0.0060	3.8797	0.0040	11.7665	0.0083	9.8471	0.0070	32.6606	0.0176	20.3661	0.0111
7	5.3834	0.0051	4.1879	0.0040	6.4355	0.0052	6.0467	0.0049	14.2092	0.0099	8.4780	0.0059
8	5.7235	0.0050	5.1996	0.0045	5.6575	0.0049	5.1996	0.0045	6.8094	0.0059	5.1996	0.0045
9	28.1374	0.0125	24.8327	0.0110	27.8865	0.0123	24.8327	0.0110	31.0905	0.0137	24.8327	0.0110
10	50.0393	0.0196	42.0273	0.0165	49.4921	0.0202	40.5529	0.0166	48.2800	0.0206	38.7968	0.0166
11	50.4156	0.0188	41.7688	0.0157	50.3536	0.0196	40.1121	0.0157	46.9718	0.0192	38.2382	0.0157
12	41.3229	0.0153	32.8000	0.0122	43.4913	0.0161	32.8000	0.0122	41.0017	0.0152	32.8000	0.0122
13	31.3867	0.0137	23.4196	0.0103	33.5648	0.0147	23.4196	0.0103	29.2538	0.0128	23.4196	0.0103
14	34.1193	0.0140	27.3522	0.0113	35.6507	0.0147	27.3522	0.0113	33.5837	0.0138	27.3522	0.0113
15	40.6447	0.0152	33.3872	0.0125	41.8699	0.0157	33.3872	0.0125	41.6449	0.0156	33.3872	0.0125
16	71.1391	0.0263	58.0524	0.0215	74.2076	0.0343	52.5962	0.0245	65.1934	0.0406	50.0200	0.0315
17	61.3569	0.0212	54.4837	0.0189	61.2155	0.0241	47.9897	0.0190	53.4560	0.0244	44.8290	0.0205
18	56.2965	0.0201	50.0568	0.0179	54.8875	0.0208	46.3598	0.0176	55.0460	0.0223	42.8049	0.0174
19	58.7210	0.0219	50.9248	0.0190	57.1217	0.0227	46.8345	0.0187	58.0300	0.0246	43.5243	0.0185
20	59.4561	0.0205	50.8888	0.0176	63.5339	0.0250	44.1462	0.0175	53.9184	0.0248	40.8728	0.0189
21	60.7259	0.0212	51.9307	0.0182	62.7859	0.0246	45.3668	0.0179	55.7654	0.0249	41.5473	0.0187
22	19.8976	0.0113	16.8151	0.0096	19.3244	0.0110	16.8151	0.0096	24.5901	0.0140	16.8151	0.0096
23	8.5649	0.0069	6.8410	0.0056	8.8973	0.0069	7.1794	0.0056	12.2951	0.0092	7.6012	0.0057
24	7.8970	0.0073	5.5832	0.0052	12.2771	0.0083	11.6368	0.0078	32.1939	0.0169	19.4013	0.0102

TABLE 11. Results of different algorithms.

Algorithm	Open switches	Active power loss (kWh)	Load balancing index (p.u)	Maximum node voltage deviation (p.u)	Fitness value1	Fitness value 2
LDBAS	45 24 6 40 47 57 28 89 70 85 76 80 100 113 33	9851.9879	2.4137	1.0813	0.00676	0.00668
CDBAS	45 24 120 53 31 55 4 63 66 85 76 81 101 116 28	9985.7243	2.5404	1.0714	0.00642	0.00615
BAS	42 12 21 51 47 60 39 95 69 73 76 82 130 109 34	10122.3608	2.5779	1.4210	0.01088	0.01099
PSO	42 24 23 51 47 59 38 95 71 87 76 107 85 109 34	10114.4309	2.5996	1.5661	0.01091	0.01161
GA	25 15 21 53 48 59 39 95 71 74 97 82 85 108 32	10248.7116	2.6110	1.5921	0.01361	0.01437

TABLE 12. Results of different algorithms.

Algorithm	The average value of objective function	The running numbers	The average convergence times	The average time/s
LDBAS	0.00692	30	140.78	1560.92
CDBAS	0.00883	27	169.01	1692.78
BAS	0.01075	12	75.77	1827.60
PSO	0.01099	6	30.04	1821.53
GA	0.01286	6	35.25	1873.81

3) EFFICIENCY VERIFICATION OF THE PROPOSED RECONFIGURATION MODEL

Now, based on the above simulation analysis, we choose the IEEE 33-bus distribution system with EV access under the smart charging/discharging pattern to verify the effectiveness of the proposed reconfiguration model. Table 10 and Fig. 11 show the actual operation modes and topological solutions under the proposed reconfiguration model over 24 hours with different levels of EV penetration. Here, we set a threshold of $\lambda_g = 0.003$. The open branches of the distribution network as determined by the LDBAS algorithm in the OR mode with EV penetration rates of 0.25, 0.5 and 0.9 are [33, 12, 11, 36, 28], [7, 9, 8, 36, 26] and [33, 10, 21, 32, 28], respectively. As seen from the results in Fig. 10, the topology of the network is changed 3, 2 and 4 times, respectively, with the proposed reconfiguration method.

Similarly, Fig. 12 shows the results for the total active power loss, the total load balancing index, the total voltage

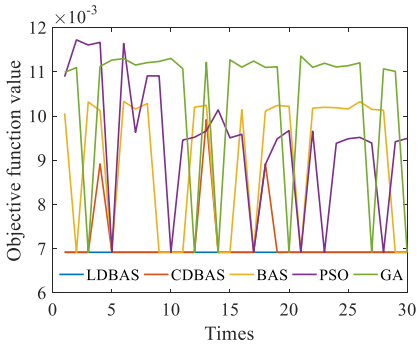

FIGURE 13. The optimal solutions found by different algorithms in 30 independent runs.

deviation index and the minimum voltage value. It is clearly seen that the minimum voltage values in the distribution network over 24 hours with EV penetration rates of 0.25, 0.5 and 0.9 that are achieved with the proposed reconfiguration method are more stable than those in the other reconfiguration modes. Moreover, the minimum voltage value obtained with the proposed reconfiguration method is the highest with an EV penetration rate of 0.5 during the peak load period between 8:00 and 22:00.

From the results for the total active power loss, the total load balancing index, and the total voltage deviation index in Fig. 11, we can find that the proposed reconfiguration method can improve power quality and reduce power loss. In particular, with an EV penetration rate of 0.9, the total active power losses in the original system, under the proposed reconfiguration method, in the OR mode and in the RTR mode are 1143.4600 kWh, 807.2915 kWh, 905.5837 kWh and 709.7367 kWh, respectively. Under the proposed reconfiguration method, the total power loss is reduced by 11.93% compared to that in the original system, indicating that the proposed method can improve the influence of EV penetration in the distribution network. In the RTR mode, although the total power loss is decreased by 97.5548 kWh, the number of switching operations is also greater than that under the proposed reconfiguration method. Thus, considering the overall operation economy in terms of network loss and switching operations, the proposed reconstruction model is superior to the RTR mode.

B. 118-BUS TEST SYSTEM

The IEEE 118-bus system consists of 118 buses and 15 tie branches [19] and operates at 11 kV. The open branches in the initial network are 119, 120, 121, 122, 123, 124, 125, 126, 127, 128, 129, 130, 131, 132 and 133. Table 6 shows the specific parameters and locations for DG and EV access. Additionally, the network parameters are given [19]. First, the IEEE 118-node system is used to simulate several pre-set scenarios to analyse the effects of different levels of EV penetration on the network. The proposed reconfiguration model is then validated on the modified IEEE 118-bus system with EV penetration rates of 0.25 and 0.5 by using the proposed LDBAS algorithm to solve the model.

1) VALIDATION OF THE LDBAS ALGORITHM

To verify the further effectiveness of the LDBAS algorithm for solving the distribution network reconfiguration problem, the IEEE 118-bus system is used for testing in scenario 1, and the BAS algorithm, the chaos disturbed beetle antennae search (CDBAS) algorithm, the PSO algorithm and a genetic algorithm (GA) are compared in accordance with the simulated OR results over 24 hours.

Table 11 shows the optimal solutions obtained with the different algorithms. Compared with the CDBAS, BAS, PSO, and GA solutions, it is clear that the solutions found by

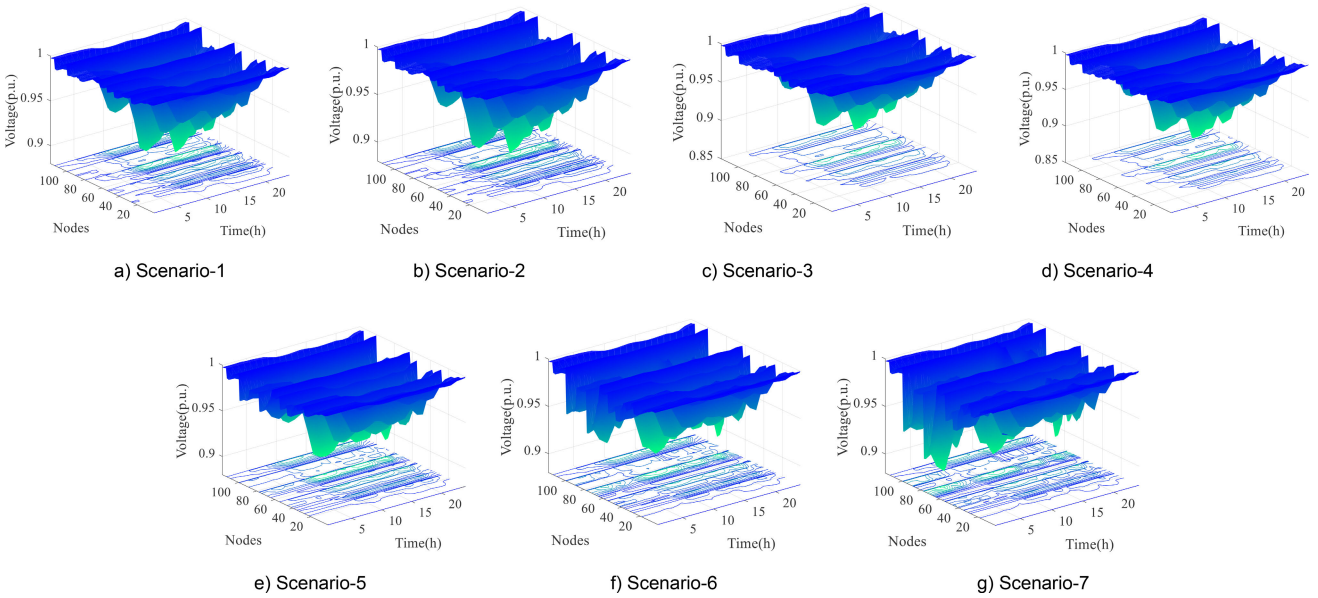

FIGURE 14. Voltage profiles of the 118-bus network with DG over 24 hours under different levels of EV penetration.

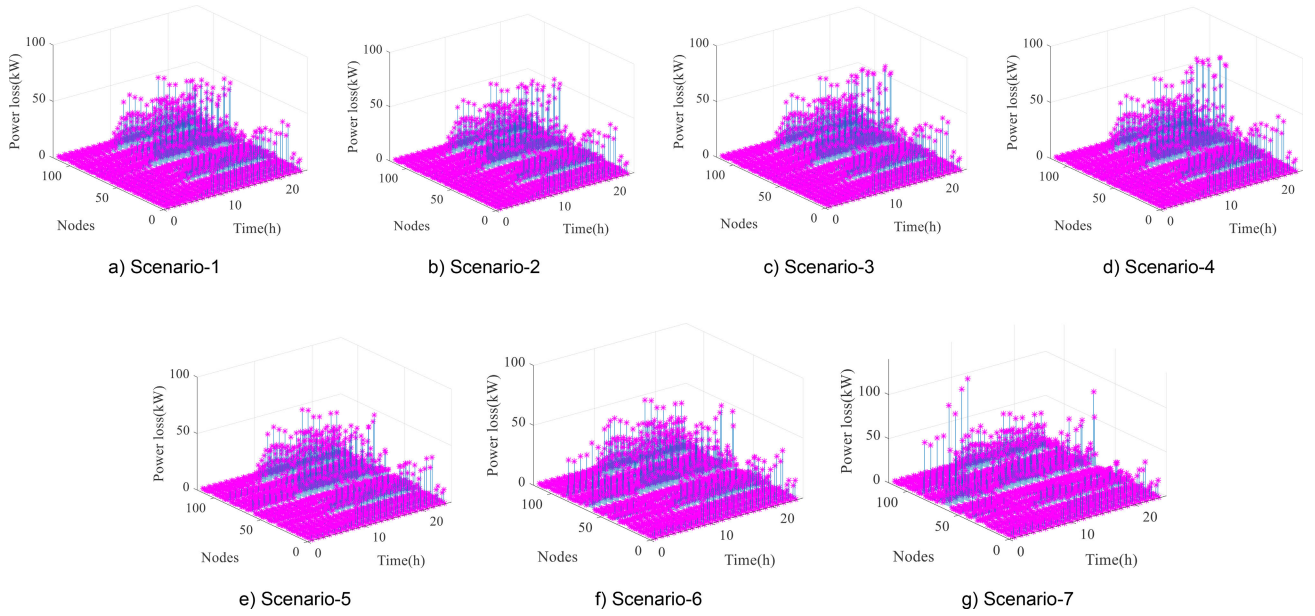

FIGURE 15. Power loss profiles of the 118-bus network with DG over 24 hours under different levels of EV penetration.

the LDBAS are best both in terms of the results for fitness value and in terms of the results for active power loss, load balancing and maximum node voltage deviation in Table 11, which further verifies the effectiveness and scalability of the proposed algorithm.

To illustrate the randomness of the intelligent algorithms, Fig. 13 shows the optimal solution curves for the LDBAS algorithm, the CDBAS algorithm, the BAS algorithm, the PSO algorithm and the GA in 30 independent runs.

Compared with the 33-bus distribution system in Table 9, the calculation time of the proposed algorithm for solving the optimization problem of the 118-bus distribution system reconfiguration is slightly increased in Table 12. Further, from the results in Table 12, it is clear that the average value of the objective function, the number of optimal solutions, the average convergence times and the average time of the LDBAS algorithm are better than those of the other four algorithms. Especially, the running numbers of the optimal solution are obtained with LDBAS algorithm is 30 times. In contrast, the running numbers of other algorithms is 27, 12, 6 and 6 times, respectively. In a word, the search efficiency of the proposed algorithm applied to the reconstruction problem of 33-bus distribution system is the same as that applied to 118-bus distribution system, which shows the stability of the proposed algorithm can be guaranteed with the complexity of the system.

2) INFLUENCE OF DIFFERENT LEVELS OF EV PENETRATION FOR A DISTRIBUTION SYSTEM WITH DG

Fig. 14 shows the voltage profiles of the 118-bus network with DG over 24 hours under different levels of EV penetration. In terms of the overall voltage profile, we can clearly see that the voltage of the distribution network with EVs under the random charging pattern is decreased compared to scenario 1 without EVs, and the voltage continues to drop as the penetration of EVs increases. However, compared with scenarios 1, 2, 3 and 4, the voltage of the network is improved under the smart EV charging/discharging pattern, as in scenarios 5, 6 and 7. From a local perspective on the voltage profile, the minimum voltage magnitudes in scenarios 1-7 are 0.8850 p.u. for node 77 at 16:00, 0.8814 p.u. for node 77 at 16:00, 0.8780 p.u. for node 77 at 16:00, 0.8735 p.u. for node 77 at 16:00, 0.8993 p.u. for node 77 at 22:00, 0.8993 p.u. for node 77 at 22:00, and 0.8967 p.u. for node 77 at 4:00, respectively. As the EV penetration rate increases, the minimum voltage value in the network first increases and then slightly decreases.

Fig. 15 shows the power loss profiles of the 118-bus network with DG over 24 hours under different levels of EV penetration. Regarding the overall power loss profile, the total active power losses in scenarios 1-7 are 12485.9022 kWh, 12865.1387 kWh, 13275.5074 kWh, 13813.6237 kWh, 12243.2257 kWh, 12792.8637 kWh, and 14065.8189 kWh, respectively. In other words, compared with the total active power losses of the network without EVs and with the smart EV charging/discharging pattern, the total active power losses under the random charging pattern, as in scenarios 1, 2, 3 and 4, are increased and continue to increase with increasing EV penetration. Moreover, the total power losses for the 118-bus distribution network with EV penetration rates of 0.25 and 0.5 are obviously reduced compared to those without EVs and with EVs under the random charging pattern. However, the total power loss of the system with an EV penetration rate of 0.8 is the highest among the seven scenarios.

TABLE 13. Actual operation mode with the proposed reconfiguration method for the 118-bus system under the smart charging/discharging pattern.

Hour	OR mode with EV penetration 0.5		RTR mode with EV penetration 0.25		OR mode with EV penetration 0.5		RTR mode with EV penetration 0.5	
	Power Loss (kW) /PLR		Power Loss (kW) /PLR		Power Loss (kW) /PLR		Power Loss (kW) /PLR	
1	101.7409	0.0133	98.6427	0.01289	209.4347	0.0255	209.3626	0.02548
2	99.2148	0.0129	91.5547	0.01189	197.2067	0.0240	201.1895	0.02443
3	104.3296	0.0144	106.3254	0.01471	225.3241	0.0289	231.9550	0.02968
4	99.5124	0.0158	100.3602	0.01597	229.0453	0.0333	238.3360	0.03457
5	96.8627	0.0127	96.2097	0.01263	151.3460	0.0191	161.1897	0.02029
6	110.4394	0.0137	111.6023	0.01382	190.2863	0.0224	215.2162	0.02528
7	111.3285	0.0123	120.0517	0.01322	139.3722	0.0151	5.1925	0.00057
8	135.2242	0.0129	140.4978	0.01338	137.0847	0.0131	140.4978	0.01338
9	319.1255	0.0204	74.2883	0.00484	321.1410	0.0206	74.2883	0.00484
10	556.3703	0.0292	127.0078	0.00681	530.4486	0.0280	182.4608	0.00980
11	621.4873	0.0304	87.0080	0.00437	590.3879	0.0290	36.8961	0.00187
12	629.2821	0.0304	108.2091	0.00537	627.3961	0.0305	108.2091	0.00540
13	569.1965	0.0296	52.8584	0.00282	565.9684	0.0296	52.8584	0.00284
14	489.4377	0.0271	43.6149	0.00247	487.9494	0.0273	43.6149	0.00250
15	535.4755	0.0280	72.3046	0.00388	535.0412	0.0284	72.3046	0.00393
16	604.4543	0.0290	56.0981	0.00276	517.4235	0.0255	814.5032	0.03949
17	683.3427	0.0299	106.4122	0.00478	614.6023	0.0273	569.0719	0.02534
18	675.8072	0.0296	19.0344	0.00086	643.1856	0.0284	97.5309	0.00441
19	634.5922	0.0294	3.3495	0.00016	601.9630	0.0281	106.9146	0.00510
20	495.3532	0.0235	113.0247	0.00545	456.4726	0.0220	366.0171	0.01769
21	650.7669	0.0281	113.2332	0.00501	600.5816	0.0263	518.9451	0.02280
22	677.3562	0.0309	30.3526	0.00143	682.1017	0.0311	30.3526	0.00143
23	238.9904	0.0164	305.7634	0.02094	253.6074	0.0174	213.3128	0.01466
24	188.3900	0.0164	3.1936	0.00028	273.2257	0.0230	3.2121	0.00028

3) EFFICIENCY VERIFICATION OF THE PROPOSED RECONFIGURATION MODEL

To verify the effectiveness and scalability of the proposed reconfiguration model, the IEEE 118-bus distribution system is selected with EV penetration rates of 0.25 and 0.5 under the smart charging/discharging pattern. Table 13 and Fig. 16 show the actual operation modes and topological solutions under the proposed reconfiguration model over 24 hours with different levels of EV penetration. Here, we set a threshold $\lambda_g = 0.006$. The open branches of the distribution network as determined by the LDBAS algorithm in the OR mode with EV penetration rates of 0.25 and 0.5 are [43, 26, 21, 53, 47, 58, 39, 95 70, 74, 98, 82, 85, 109, 33] and [42, 26, 20, 52, 47, 58, 39, 95, 72, 74, 76, 81, 85, 109, 33], respectively. As seen from the results in Fig. 16, the topology of the network with EV penetration rates of 0.25 and 0.5 is changed 2 and 4 times, respectively, with the proposed reconfiguration method.

Fig. 17 shows the results for the minimum voltage value in the 118-bus network over 24 hours. It is clearly seen that the minimum voltage values in the distribution network over 24 hours with EV penetration rates of 0.25 and 0.5 are significantly improved by the proposed reconfiguration method compared with the minimum voltage value in the original system. Although the minimum voltage values obtained with the proposed method are not as good as those obtained with the RTR method, they are more stable over 24 hours.

Fig. 17 also shows the results for the total active power loss, the total load balancing index and the total voltage deviation index. The total active power losses in the 118-bus network with the proposed reconfiguration method and in the RTR mode are decreased by 76.1501% and 82.1861%,

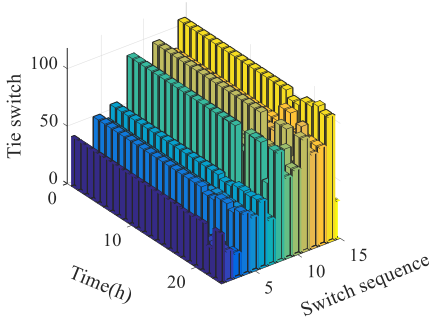

a) Distribution system with an EV penetration rate of 0.25

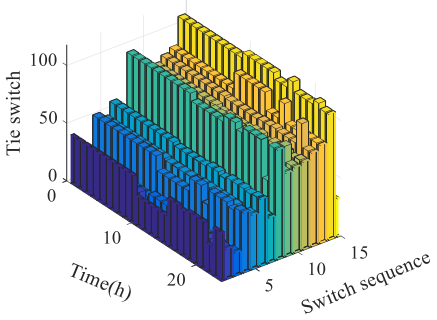

b) Distribution system with an EV penetration rate of 0.5

FIGURE 16. Switch states over 24 hours as determined with the proposed reconfiguration model under the smart charging/discharging pattern.

respectively, for an EV penetration rate of 0.25 and by 58.3731% and 63.3121%, respectively, for an EV penetration rate of 0.5. Thus, considering the large number of topological updates and the slight percentage reduction in the total power loss in the RTR mode, the proposed reconstruction method is more effective for optimizing the reconfiguration of the distribution network in terms of economy. In addition, compared

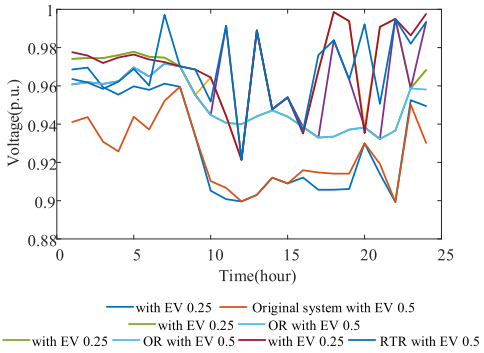

a) Minimum voltage profile

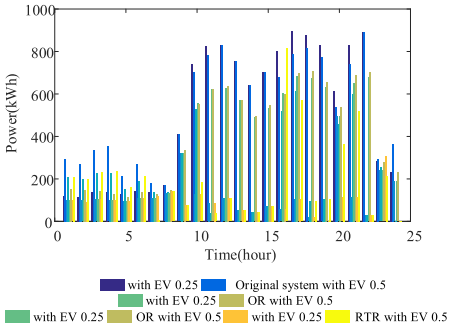

b) Total power loss profile

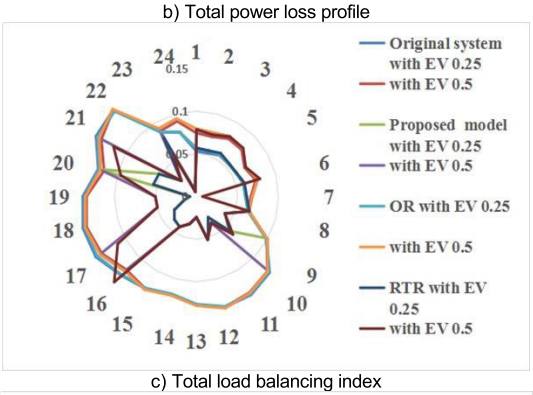

c) Total load balancing index

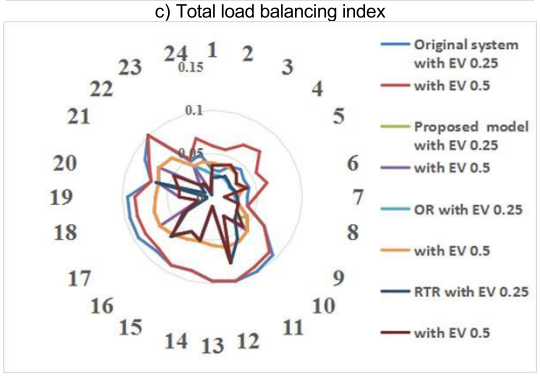

d) Total voltage deviation index

FIGURE 17. Results of the proposed reconfiguration method for the 118-bus network over 24 hours.

with the other reconfiguration modes, the total load balancing index and the total voltage deviation index achieved with the proposed reconfiguration method are more stable and closer to the centre of the circle, indicating that the proposed method can improve the power quality.

VII. CONCLUSION

A dynamic reconfiguration method based on the power loss rate (PLR) is presented considering variations in load and distributed generation (DG) outputs and different levels of electric vehicle (EV) penetration. The objective functions of the reconfiguration model include the power loss, the load balancing index and the node voltage deviation index to ensure operation economy and improve the power quality in the system. Additionally, an improved Lévy flight and chaos disturbed beetle antennae search (LDBAS) algorithm, which offers increased calculation speed, is applied to the model to find the optimal reconfiguration (OR) solution for the distribution network.

Furthermore, the effectiveness of the proposed LDBAS algorithm and the superiority of the proposed dynamic reconstruction model are validated on the modified IEEE 33 and 118-bus systems. First, compared with other algorithms, the LDBAS algorithm is superior in terms of its global search ability, calculation speed and robustness for finding the OR solution for the distribution network; accordingly, it can also be considered for solving optimization problems for scheduling strategies considering the dynamic reconfiguration of the distribution network. Second, the proposed reconfiguration method can improve the economic performance and power quality of the system during operation more effectively than the RTR mode can. Moreover, compared with the original systems with an EV penetration rate of 0.9 under the smart charging/discharging pattern, the total power losses in the IEEE 33 and IEEE 118-bus systems are significantly reduced by the proposed reconfiguration method. Therefore, the presented dynamic reconstruction method can enhance the effects of EVs and thus encourage EV penetration in distribution systems

REFERENCES

[1] A. S. Dobakhshari and M. Fotuhi-Firuzabad, "A reliability model of large wind farms for power system adequacy studies," *IEEE Trans. Energy Convers.*, vol. 24, no. 3, pp. 792–801, Sep. 2009, doi: 10.1109/TEC.2009.2025332.

[2] L. H. Yang and Z. Xu, "Electric vehicles in Danish power system with large penetration of wind power," *Autom. Electr. Power Syst.*, vol. 35, no. 14, pp. 43–47, Jul. 2011.

[3] B. Amanulla, S. Chakrabarti, and S. N. Singh, "Reconfiguration of power distribution systems considering reliability and power loss," *IEEE Trans. Power Del.*, vol. 27, no. 2, pp. 918–926, Apr. 2012, doi: 10.1109/TPWRD.2011.2179950.

[4] S. K. Goswami and S. K. Basu, "A new algorithm for the reconfiguration of distribution feeders for loss minimization," *IEEE Trans. Power Del.*, vol. 7, no. 3, pp. 1484–1491, Jul. 1992, doi: 10.1109/61.141868.

[5] J. Wen, Y. Tan, L. Jiang, and K. Lei, "Dynamic reconfiguration of distribution networks considering the real-time topology variation," *IET Gener., Transmiss. Distrib.*, vol. 12, no. 7, pp. 1509–1517, Apr. 2018, doi: 10.1049/iet-gtd.2017.1304.

[6] M. Hemmati, B. Mohammadi-Ivatloo, M. Abapour, and A. Anvari-Moghaddam, "Day-ahead profit-based reconfigurable microgrid scheduling considering uncertain renewable generation and load demand in the presence of energy storage," *J. Energy Storage*, vol. 28, Apr. 2020, Art. no. 101161, doi: 10.1016/j.est.2019.101161.

[7] L. Y. Yin and J. L. Yu, "Dynamic reconfiguration of distribution network with multi-time period," *Proc. CSEE*, vol. 22, no. 7, pp. 44–48, Jul. 2002.

[8] S. Esmaeili, A. Anvari-Moghaddam, S. Jadid, and J. M. Guerrero, "Optimal simultaneous day-ahead scheduling and hourly reconfiguration of distribution systems considering responsive loads," *Int. J. Electr. Power Energy Syst.*, vol. 104, pp. 537–548, Jan. 2019, doi: 10.1016/j.ijepes.2018.07.055.

[9] Y.-Y. Hong and Y.-F. Luo, "Optimal VAR control considering wind farms using probabilistic load-flow and gray-based genetic algorithms," *IEEE Trans. Power Del.*, vol. 24, no. 3, pp. 1441–1449, Jul. 2009, doi: 10.1109/TPWRD.2009.2016625.

[10] J. X. Zhao, H. N. Niu, and Y. Z. Wang, "Dynamic reconfiguration of active distribution network based on information entropy of time intervals," *Power Syst. Technol.*, vol. 41, no. 2, pp. 402–408, Feb. 2017.

[11] M.-H. Shariatkhah, M.-R. Haghifam, J. Salehi, and A. Moser, "Duration based reconfiguration of electric distribution networks using dynamic programming and harmony search algorithm," *Int. J. Electr. Power Energy Syst.*, vol. 41, no. 1, pp. 1–10, Oct. 2012, doi: 10.1016/j.ijepes.2011.12.014.

[12] Z. Liu, Y. Liu, G. Qu, X. Wang, and X. Wang, "Intra-day dynamic network reconfiguration based on probability analysis considering the deployment of remote control switches," *IEEE Access*, vol. 7, pp. 145272–145281, 2019, doi: 10.1109/ACCESS.2019.2944917.

[13] T. Hao, L. Ü. Lin, G. A. Hongjun, L. Min, W. Gang, C. Siqi, and Z. Xin, "Dynamic reconfiguration of distribution network considering power grid operation characteristic," *Power Syst. Protection Control*, vol. 43, no. 1, p. 9G14, Jan. 2015.

[14] C. Wang, S. Lei, P. Ju, C. Chen, C. Peng, and Y. Hou, "MDP-based distribution network reconfiguration with renewable distributed generation: Approximate dynamic programming approach," *IEEE Trans. Smart Grid*, vol. 11, no. 4, pp. 3620–3631, Jul. 2020, doi: 10.1109/TSG.2019.2963696.

[15] D. S. Rani, N. Subrahmanyam, and M. Sydulu, "Multi-Objective invasive weed optimization—An application to optimal network reconfiguration in radial distribution systems," *Int. J. Electr. Power Energy Syst.*, vol. 73, pp. 932–942, Jul. 2015, doi: 10.1016/j.ijepes.2015.06.020.

[16] M.-S. Tsai and F.-Y. Hsu, "Application of grey correlation analysis in evolutionary programming for distribution system feeder reconfiguration," *IEEE Trans. Power Syst.*, vol. 25, no. 2, pp. 1126–1133, May 2010.

[17] H. M. Khodr and J. Martinez-Crespo, "Integral methodology for distribution systems reconfiguration based on optimal power flow using benders decomposition technique," *IET Gener., Transmiss. Distrib.*, vol. 3, no. 6, pp. 521–534, Jun. 2009, doi: 10.1049/iet-gtd.2008.0289.

[18] C. Gerez, L. I. Silva, E. A. Belati, A. J. Sguarezi Filho, and E. C. M. Costa, "Distribution network reconfiguration using selective firefly algorithm and a load flow analysis criterion for reducing the search space," *IEEE Access*, vol. 7, pp. 67874–67888, 2019.

[19] M. A. Samman, H. Mokhlis, N. N. Mansor, H. Mohamad, H. Suyono, and N. M. Sapari, "Fast optimal network reconfiguration with guided initialization based on a simplified network approach," *IEEE Access*, vol. 8, pp. 11948–11963, 2020, doi: 10.1109/ACCESS.2020.2964848.

[20] A. Y. Abdelaziz, F. M. Mohamed, S. F. Mekhamer, and M. A. L. Badr, "Distribution system reconfiguration using a modified tabu search algorithm," *Electr. Power Syst. Res.*, vol. 80, no. 8, pp. 943–953, Aug. 2010.

[21] B. D. Zhang and Y. Liu, "A distribution network reconfiguration algorithm based on evolutionary programming mutation operator," *Power Syst. Technol.*, vol. 36, no. 4, pp. 202–206, 2012.

[22] T. T. Nguyen and T. T. Nguyen, "An improved cuckoo search algorithm for the problem of electric distribution network reconfiguration," *Appl. Soft Comput.*, vol. 84, Nov. 2019, Art. no. 105720, doi: 10.1016/j.asoc.2019.105720.

[23] H. D. de Macedo Braz and B. Alencar de Souza, "Distribution network reconfiguration using genetic algorithms with sequential encoding: Subtractive and additive approaches," *IEEE Trans. Power Syst.*, vol. 26, no. 2, pp. 582–593, May 2011, doi: 10.1109/TPWRS.2010.2059051.

[24] R. Tuladha, J. Singh, and W. Ongsakul, "A multi-objective network reconfiguration of distribution network with solar and wind distributed generation using NSPSO," in *Proc. Int. Conf. Green Energy Sustain. Develop.*, Cape Town, South Africa: IEEE, Mar. 2014, pp. 1–7.

[25] M.-R. Andervazh, M.-R. Haghifam, and J. Olamaei, "Adaptive multi-objective distribution network reconfiguration using multi-objective discrete particles swarm optimisation algorithm and graph theory," *IET Gener., Transmiss. Distrib.*, vol. 7, no. 12, pp. 1367–1382, Dec. 2013, doi: 10.1049/iet-gtd.2012.0712.

[26] K. Prasad, R. Ranjan, N. C. Sahoo, and A. Chaturvedi, "Optimal reconfiguration of radial distribution systems using a fuzzy mutated genetic algorithm," *IEEE Trans. Power Del.*, vol. 20, no. 2, pp. 1211–1213, Apr. 2005, doi: 10.1109/TPWRD.2005.844245.

[27] N. Gupta, A. Swarnkar, K. R. Niazi, and R. C. Bansal, "Multi-objective reconfiguration of distribution systems using adaptive genetic algorithm in fuzzy framework," *IET Gener. Trans. Distrib.*, vol. 4, no. 12, pp. 1288–1298, 2010, doi: 10.1049/iet-gtd.2010.0056.

[28] A. M. Eldurssi and R. M. O'Connell, "A fast nondominated sorting guided genetic algorithm for multi-objective power distribution system reconfiguration problem," *IEEE Trans. Power Syst.*, vol. 30, no. 2, pp. 593–601, Mar. 2015, doi: 10.1109/TPWRS.2014.2332953.

[29] A. Jafari, H. G. Ganjehlou, F. B. Darbandi, B. Mohammadi-Ivatloo, and M. Abapour, "Dynamic and multi-objective reconfiguration of distribution network using a novel hybrid algorithm with parallel processing capability," *Appl. Soft Comput.*, vol. 90, May 2020, Art. no. 106146, doi: 10.1016/j.asoc.2020.106146.

[30] M. Esmaeili, M. Sedighizadeh, and M. Esmaili, "Multi-objective optimal reconfiguration and DG (distributed generation) power allocation in distribution networks using big bang-big crunch algorithm considering load uncertainty," *Energy*, vol. 103, pp. 86–99, May 2016, doi: 10.1016/j.energy.2016.02.152.

[31] M. A. T. G. Jahani, P. Nazarian, A. Safari, and M. R. Haghifam, "Multi-objective optimization model for optimal reconfiguration of distribution networks with demand response services," *Sustain. Cities Soc.*, vol. 47, May 2019, Art. no. 101514, doi: 10.1016/j.scs.2019.101514.

[32] T. S. Ustun, S. M. S. Hussain, and H. Kikusato, "IEC 61850-based communication modeling of EV charge-discharge management for maximum PV generation," *IEEE Access*, vol. 7, pp. 4219–4231, 2019, doi: 10.1109/ACCESS.2018.2888880.

[33] W. Kempton and S. E. Letendre, "Electric vehicles as a new power source for electric utilities," *Transp. Res. Part D, Transp. Environ.*, vol. 2, no. 3, pp. 157–175, Sep. 1997.

[34] X. Jiang and S. Li, "BAS: Beetle antennae search algorithm for optimization problems," 2017, *arXiv:1710.10724*. [Online]. Available: http://arxiv.org/abs/1710.10724

[35] A. A. Heidari and P. Pahlavani, "An efficient modified grey wolf optimizer with Lévy flight for optimization tasks," *Apply Softw. Comput.*, vol. 60, pp. 1315–1341, Nov. 2017, doi: 10.1016/j.asoc.2017.06.044.

[36] M. Z. Ali, N. H. Awad, R. G. Reynolds, and P. N. Suganthan, "A balanced fuzzy cultural algorithm with a modified Lévy flight search for real parameter optimization," *Inf. Sci.*, vol. 447, pp. 351–352, Jun. 2018, doi: 10.1016/j.ins.2018.03.008.

[37] B. Li and W. S. Jiang, "Chaos optimization method and its application," *Control Theory Appl.*, no. 4, pp. 613–615, 1997.

[38] Y. G. Dong and S. F. Liu, *Grey System Theory and Its Application*. Beijing, China: Science Press, 2014, pp. 256–261.

[39] Y. Li, Y. Li, G. Li, D. Zhao, and C. Chen, "Two-stage multi-objective OPF for AC/DC grids with VSC-HVDC: Incorporating decisions analysis into optimization process," *Energy*, vol. 147, pp. 286–296, Mar. 2018, doi: 10.1016/j.energy.2018.01.036.

[40] Y. Li, J. Wang, D. Zhao, G. Li, and C. Chen, "A two-stage approach for combined heat and power economic emission dispatch: Combining multi-objective optimization with integrated decision making," *Energy*, vol. 162, pp. 237–254, Nov. 2018, doi: 10.1016/j.energy.2018.07.200.

[41] J. Wang, W. Wang, Z. Yuan, H. Wang, and J. Wu, "A chaos disturbed beetle antennae search algorithm for a multiobjective distribution network reconfiguration considering the variation of load and DG," *IEEE Access*, vol. 8, pp. 97392–97407, 2020, doi: 10.1109/ACCESS.2020.2997378.

[42] N. Xiong and H. Z. Cheng, "Switch group-based tabu algorithm applied in distribution network dynamic reconfiguration," *Autom. Electr. Power Syst.*, vol. 32, no. 11, pp. 56–60, 2008.

JIE WANG received the B.E. and M.E. degrees in electric power systems and automation from Xinjiang University, Urumqi, China, in 2014 and 2018, respectively, where she is currently pursuing the Ph.D. degree with the Engineering Research Center of Renewable Energy Power Generation and Grid-Connected Control, Ministry of Education. Her current research interests include the control of renewable energy power generation and smart grid technology.

WEIQING WANG received the B.E. degree in electric power systems and automation from the Xinjiang Institute of Technology, Urumqi, China, in 1983, and the M.E. degree in electric power systems and automation from Zhejiang University, Hangzhou, China, in 1990. He is currently a Professor with the Engineering Research Center of Renewable Energy Power Generation and Grid-connected Control, Ministry of Education, Xinjiang University. His current research interests include the control of renewable energy power generation and smart grid technology.

HAIYUN WANG received the B.E. degree in electric power systems and automation from Xinjiang University, Urumqi, China, in 1995, and the M.E. degree in electrical engineering from the Dalian University of Technology, Liaoning, China, in 1999. She is currently a Professor with the Engineering Research Center of Renewable Energy Power Generation and Grid-connected Control, Ministry of Education, Xinjiang University. Her current research interests include the control of renewable energy power generation and smart grid technology.

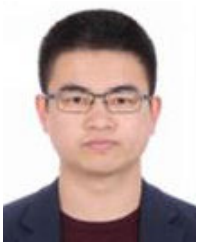

HUIWEN ZUO received the B.E. degree in measurement and control technology and instrumentation program from Beihang University, Beijing, China, in 2013, and the M.E. degree in electrical engineering from Xinjiang University, Urumqi, China, in 2018. He is currently an Engineer with the Shanghai Research Institute of Aerospace Computer Technology. His current research interests include the control of renewable energy power generation and ground-based radiometer technology.